24 Hills Road, **P** 01223 855346
Cambridge **W** elifesciences.org
CB2 1JP **T** @elife_sciences

A silicon nanomembrane-based *in vitro* platform to visualize immune cell trafficking across the human blood-brain barrier

Tracking no: 20-04-2018-ISTR-eLife-37743

Britta Engelhardt (University of Bern)

Abstract:
Here we report on the development of a breakthrough **micro**fluidic human *in vitro* **cerebrovascular barrier (CVB)** model featuring stem cell derived brain like endothelial cells (BLECs) and nanoporous **si**licon nitride (NPN) **m**embranes (µSiM-CVB). Nanoscale thinness of NPN membranes combined with their high permeability and mechanical stability make them an ideal scaffold for the assembly of an *in vitro* microfluidic model of the blood-brain barrier (BBB) featuring cellular elements of the neurovascular unit (NVU). Dual-chamber devices divided by NPN membranes yield tight barrier properties in BLECs, and allow an abluminal pericyte-co-culture to be replaced with pericyte-conditioned media. With the benefit of physiological flow and superior imaging quality, our µSiM-CVB captures each phase of the multi-step T-cell migration across the BBB. The small volume of < 100 µL of the µSiM-CVB will enable *in vitro* investigations of rare patient derived immune cells with the human BBB by live cell imaging under flow.

Impact statement:

Competing interests: No competing interests declared

Author contributions:

Funding:
Swiss National Science Foundation; NIH; Swiss Multiple Sclerosis Society; Germain de Stael

Data Availability:
N/A
N/A

Ethics:

Author Affiliation:
Britta Engelhardt(Theodor Kocher Institute,University of Bern,Switzerland)

Dual-use research: N/a

Permissions: Have you reproduced or modified any part of an article that has been previously published or submitted to another journal? N/A

A silicon nanomembrane-based *in vitro* platform to visualize immune cell trafficking across the live human blood-brain barrier

Adrien Mossu[1#], Maria Rosito[1#], Tejas Khire[2], Hung Li Chung[2], Hideaki Nishihara[1], Isabelle Gruber[1], Emma Luke[2], Lucie Dehouck[5], Federica Sallusto[3,4], Fabien Gosselet[5], James McGrath[2]*, Britta Engelhardt[1]*

[1]Theodor Kocher Institute, University of Bern, Switzerland; [2]Department of Biomedical Engineering, University of Rochester, Rochester, NY, USA, [3]Institute for Research in Biomedicine, Bellinzona, Switzerland, [4]Institute for Microbiology, ETH Zurich, Zurich, Switzerland and [5]Blood Brain Barrier Laboratory, University of Artois, Lens, France.

[#] equal contribution

Running title: A novel microfluidic human *in vitro* cerebrovascular barrier (CVB)

Keywords: blood-brain barrier, microfluidics, nanoporous silicon nitride membrane, two-compartmental flow chamber, T-cell migration

***Shared correspondence:**

Dr. Britta Engelhardt
Theodor Kocher Institute
University of Bern
Switzerland
E-Mail: bengel@tki.unibe.ch

Tel. + 41 31 631 4143

Dr. James McGrath
Department of Biomedical Engineering
University of Rochester, Rochester, NY
USA
jmcgrath@bme.rochester.edu

+ 1- 585-273-5489

Abstract

Here we report on the development of a breakthrough **micro**fluidic human *in vitro* **cerebrovascular barrier (CVB)** model featuring stem cell derived brain like endothelial cells (BLECs) and nanoporous **si**licon nitride (NPN) **m**embranes (µSiM-CVB). The nanoscale thinness of NPN membranes combined with their high permeability and mechanical stability make them an ideal scaffold for the assembly of an *in vitro* microfluidic model of the blood-brain barrier (BBB) featuring cellular elements of the neurovascular unit (NVU). Dual-chamber devices divided by NPN membranes yield tight barrier properties in BLECs, and allow an abluminal pericyte-co-culture to be replaced with pericyte-conditioned media. With the benefit of physiological flow and superior imaging quality, our µSiM-CVB captures each phase of the multi-step T-cell migration across the BBB. The small volume of < 100 µL of the µSiM-CVB will enable *in vitro* investigations of rare patient derived immune cells with the human BBB by live cell imaging under flow.

Introduction

The endothelial blood-brain barrier (BBB) in central nervous system (CNS) parenchymal microvessels protects the CNS from the constantly changing milieu in the blood stream. In addition to strictly controlling the movement of molecules across its interfaces it also rules the entry of immune cells and immune mediators into the CNS (Engelhardt & Ransohoff, 2012). Under physiological conditions, immune cell entry into the CNS is very low. In contrast, in CNS inflammatory diseases such as multiple sclerosis (MS) high numbers of immune cells infiltrate the CNS, where they cause inflammation, BBB dysfunction and demyelination (Sospedra & Martin, 2016). Immune cell trafficking across the BBB is thus a critical hallmark of MS (Diebold & Derfuss, 2016) and has been extensively studied in experimental autoimmune encephalomyelitis (EAE), an animal model for multiple sclerosis (Krishnamoorthy & Wekerle, 2009). *In vitro* and *in vivo* live cell imaging studies in rodents suffering from EAE have provided evidence that T-cell migration across the BBB is a multi-step process, where T cells start to roll on the endothelial surface and after their arrest, crawl against the direction of the blood flow to sites permissive of T-cell diapedesis across the BBB (summarized in (Engelhardt & Ransohoff, 2012). α4-integrins on the T cells were identified

to mediate their arrest to the BBB in the absence or presence of autoimmune neuroinflammation in rodent EAE models, and antibodies blocking α4-integrins were shown in a variety of EAE models to inhibit the development of clinical symptoms (Engelhardt & Ransohoff, 2012). These findings were successfully translated into the clinic, where the humanized monoclonal anti- α4-integrin antibody natalizumab is used for the treatment of MS (Diebold & Derfuss, 2016). Unfortunately, natalizumab comes with the unforeseen and rare side effect of progressive multifocal leukoencephalopathy (PML), which is caused by infection of human oligodendrocytes with the JC virus and can thus not be modeled in animals. Furthermore, a number of anti-inflammatory treatments that were highly effective in EAE, have failed in MS trials (Martin, Sospedra, Rosito, & Engelhardt, 2016), underscoring that the autoimmune pathogenesis underlying MS and its treatments cannot be modelled in their entire complexity in available animal models. Therefore, there is an unmet need for detailed functional studies employing human disease-relevant tissues and cells. This includes the necessity for human models of the BBB allowing the study of migration by disease-relevant immune cell subsets across the cellular barrier as a critical step in MS pathogenesis.

Most well-characterized BBB culture models are based on primary brain endothelial cells or brain endothelial cell lines from animal origin (bovine, porcine and murine) (Grant, Abbott, & Janigro, 1998; Helms et al., 2016; Steiner, Coisne, Engelhardt, & Lyck, 2011). Although elegant human *in vitro* BBB models employing primary human brain endothelial cells have been established (Cayrol, Haqqani, Ifergan, Dodelet-Devillers, & Prat, 2011) their availabilities are limited to few laboratories with privileged access to human brain tissue. Thus, human brain endothelial cell lines like the hCMEC/D3 have been established and widely used as *in vitro* models of the human BBB (Eigenmann et al., 2013; Weksler et al., 2005). Although hCMEC/D3 retain morphological and functional characteristics of human brain endothelium, they fail to establish barrier characteristics resembling their tightness observed in BBB *in vivo* (Deli, Abraham, Kataoka, & Niwa, 2005). This limits the suitability of hCMEC/D3 for pharmacological, toxicological and functional assays on the human BBB with *in vivo* predictability.

Recently, stem cell sources have demonstrated substantial advantage over other brain endothelial cells sources for BBB modeling given their human origin, stability, scalability, self-renewal and potential to generate syngeneic cellular components of the neurovascular unit (Canfield et al., 2017; Lippmann, Al-Ahmad, Palecek, & Shusta, 2013). We have recently employed cord blood $CD34^+$ hematopoietic stem cells to differentiate endothelial cells (ECs)(Cecchelli et al., 2014). By co-culturing $CD34^+$ -derived ECs with bovine pericytes we were able to differentiate those ECs into brain-like endothelial cells (BLECs) providing a valuable *in vitro* model for the human BBB (Cecchelli et al., 2014). Growing BLECs on conventional cell culture filter inserts in co-culture with pericytes, we and others used both small molecule diffusion and transendothelial electrical resistance (Cecchelli et al., 2014; Vandenhaute et al., 2016) to establish that BLECs form tight barriers. With their excellent barrier function and robust expression of BBB signature molecules in combination with large-scale availability, BLECs are an ideal culture platform to study the interaction of human immune cells with the human BBB *in vitro* (Lyck et al., 2017).

To use BLECs in a model system to investigate immune cell interactions with the BBB, also requires a culture platform that enables live cell observations. Microscopic imaging in conventional culture inserts is severely hampered by the fact that the polymer track-etched (TE) membranes used in cell culture filter inserts are largely opaque to transmitted light and degrade fluorescence signals (Carter et al., 2017). Even the routine monitoring of confluency of the endothelial monolayers during cell culture is impaired by the incompatibility of TE membranes with phase contrast microscopy.

Live cell imaging and phase microscopy on coverglass substrates, are well-established as the means of monitoring immune cell migration across endothelial monolayers *in vitro* under static and flow conditions (Coisne, Lyck, & Engelhardt, 2013; Martinelli et al., 2014; Munir, Rainger, Nash, & McGettrick, 2015; Shulman & Alon, 2012). Following its arrest on the endothelial monolayer, an immune cell rapidly changes from a phase-bright roundish shape that can easily be distinguished from the endothelial monolayer, to a polarized cell that first spreads atop of the endothelial monolayer and then crawls along the endothelium, and then finally to a phase-dark cell as it migrates beneath the endothelial monolayer (Cinamon, Grabovsky, et al., 2001; Luu, Rainger, & Nash, 2000; Rudolph et al., 2016; Steiner et al., 2010). Similarly, live fluorescence imaging has been used to reveal the dynamics of immune cells and adhesion receptors

(Shaw et al., 2004) during their interaction with endothelial monolayers and to eventually distinguish between paracellular and transcellular routes of diapedesis (Abadier et al., 2015; Carman et al., 2007; Rudolph et al., 2016). Because glass coverslips are impermeable, these studies cannot be done in the dual chamber co-culture systems needed to establish continuous cross talk between brain microvascular endothelial cells and the pericytes and astrocytes of the neurovascular unit (Abbott, Patabendige, Dolman, Yusof, & Begley, 2010; Garberg et al., 2005).

Another critical feature of an *in vitro* model for the study of the interaction of immune cells with the BBB is the ability to maintain fluid flow during the interaction of the immune cells with the endothelial monolayer maintaining its BBB characteristics. The inability to introduce any flow in the apical and basal compartments of two chamber systems employing filter inserts limits their application to assays performed under static conditions (no shear forces). Although static BBB models have provided provisional answers to questions regarding the molecular mechanism of immune cell trafficking across the BBB (Lyck et al., 2017; Reiss, Hoch, Deutsch, & Engelhardt, 1998; Steiner et al., 2011), the physiological representation of immune cell trafficking across the BBB clearly requires the presence of flow (Cinamon, Shinder, & Alon, 2001; Schreiber, Shinder, Cain, Alon, & Sackstein, 2007; Steiner et al., 2010; Steiner et al., 2011). Several studies convincingly demonstrated that physiological shear forces influence each phase of the multi-step process including the arrest and crawling of T cells on the endothelium, and the cellular pathway of diapedesis across the endothelial monolayer (Cinamon, Shinder, et al., 2001; Schreiber et al., 2007; Steiner et al., 2011).

Here we report on the development of a novel BBB model for the study of leukocyte/BBB interactions. Ours is the first microfluidic BBB model (μSiM-CVB) to feature BLECs and the first to feature silicon nanomembranes. Silicon nanomembranes (DesOrmeaux et al., 2014; Striemer, Gaborski, McGrath, & Fauchet, 2007) are freestanding nanoporous membranes with a thicknesses (~ 100 nm) comparable to the BBB basement membrane (Kelley, Lohmer, Hagedorn, & Sherwood, 2014; Tanner, 2012). The thinness of nanomembranes makes them transparent and thus compatible with all forms of light microscopy including phase and DIC (Carter et al., 2017). The thinness of nanomembranes also gives them orders of magnitude higher permeability to small molecules than conventional membranes (Kim et al., 2008;

Striemer et al., 2007) maximizing molecular cross-talk between compartments in a co-culture system. Here we show that a µSiM-CVB device with BLECs and nanomembranes yields tight barrier properties and robust cell junctions when perfused from the abluminal side with pericyte conditioned media. This eliminates the need for pericyte or astrocyte co-culture, providing an enormous simplification. In a dual-chamber culture system with glass-like imaging quality, we show that our µSiM-CVB model captures each phase of the multi-step T-cell migration across the BBB under flow. Further, the volume of the device is small enough (< 100 µL) to facilitate investigation of rare patient derived cellular subsets with limited expansion potential. Collectively, these characteristics make our µSiM-CVB model a breakthrough platform for the study of interactions between human immune cells and the human BBB *in vitro.*

Results

Commercial supports are not suitable for live cell imaging of the human *in vitro* BBB model under physiological flow

We have previously developed a custom-made flow chamber that allowed us to observe the interaction of immune cells with an *in vitro* model of the mouse BBB established from primary mouse brain microvascular endothelial cells (pMBMECs) by live cell imaging (Coisne et al., 2013). As pMBMECs do not require co-culture conditions to establish BBB characteristics, they can be grown in petridishes with polymer coverslip bottoms, e.g. µ -dish 35mm (ibidi) allowing for high imaging quality. A custom made flow chamber can, in this case, be tightly mounted over the pMBMEC monolayers using a magnetic system (Coisne et al., 2013). For experimental conditions requiring co-culture of pMBMECs, e.g. with astrocytes, prior to live cell imaging of immune cell interaction with pMBMECs under flow, we have successfully adapted the flow chamber setup such that it allows for insertion of pMBMEC monolayers grown on commercially available filter membranes (Enzmann et al., 2013). Although this adaptation came with a reduction in imaging quality of the pMBMEC monolayer, the multi-step immune cell interaction with the pMBMEC monolayer could be investigated (Enzmann et al., 2013).

In the present study, we therefore employed our established methodology to transfer our novel human *in*

vitro model of the BBB established from $CD34^+$ derived endothelial cells (EC) (Cecchelli et al., 2014) to the established custom-made flow chamber device (Coisne et al., 2013). In order to perform the $CD34^+$ -derived EC/pericyte co-cultures necessary to establish the BBB we first tested several commercially available inserts. We first used the Milicell® standing inserts with a PTFE membrane to grow the $CD34^+$ -derived ECs. To this end $3.5x10^5$ $CD34^+$ -derived ECs were seeded on the Matrigel™ coated membrane and the co-culture with pericytes was started as described before (Cecchelli et al., 2014). Unfortunately, we could not show the BBB maturation on these filters because $CD34^+$-derived EC did not form confluent monolayers. To improve adhesive characteristics of the Millicell® PTFE filters, we tested coating with different extracellular matrix proteins and combinations thereof including Matrigel™, laminins, collagens and fibronectin. None of these coatings provided attachment of the endothelial monolayers suitable to perform flow assays, as EC readily detached upon application of flow (Supplementary video 1).

We therefore systematically tested adhesion and growth of $CD34^+$ - derived EC on additional 6 commercially available filter systems to test their optical properties and their compatibility with the cell growth: Millicell® polycarbonate, the Millicell® mixed cellulose esters, Corning polycarbonate, Corning PTFE with collagen coating, Corning PET and Greiner PET (Supplementary table 1). Although these filters all allowed for the growth of $CD34^+$ derived EC into confluent monolayers as confirmed by immunofluorescence staining of the fixed BLECs, the Millicell® membranes (polycarbonate and mixed cellulose esters) and the Corning polycarbonate membrane were not optically transparent to allow to judge the confluency of the live cell monolayer. The other three filter inserts (Corning PTFE with collagen coating, Corning PET and Greiner PET) were used to perform the flow assays. After the co-culture procedure, the filters had to be cut out of their frame and inserted into our custom-made flow chamber by placing the filter on an Ibidi μdish with the flow chamber mounted on top (Coisne et al., 2013). Cutting out the filters beared the risk of mechanical rupture of the endothelial monolayer. Also, the live cell imaging studies performed with this setup had a very low imaging quality and were not of sufficient quality for a thorough evaluation of T-cell/BBB interactions. In the assay with the Corning pre-coated PTFE filters, we were able to see the shapes of the T cells but it was impossible to clearly visualize the BLECs

(Supplementary video 2). On the PET filters from Corning (Supplementary video 3) and Greiner (Supplementary video 4) we were again not able to clearly see the BLECs and the background was too high to evaluate the behavior of the T cells even though they were visible. Thus, we concluded that we could not adapt our existing flow chamber for the study of T-cell/BLEC interactions under flow.

A thorough review of experimental microfluidic culture devices described in the literature also suggests that these would not provide ready solutions to our needs. Most generally, these systems are not amenable to live cell observations of T cell/BLEC interactions due to the lack of membrane transparency (Goncharova & Khaldoyanidi, 2013; Takeshita et al., 2014), and/or due to the fact that the endothelial cells are not grown in a single horizontal plane but vertically (Xu et al., 2016) or on the luminal surface of tubings (Cucullo et al., 2008; Herland et al., 2016; Neuhaus et al., 2006). Moreover, some of these systems employ large amounts of fluid volume to maintain flow over time (Erbeldinger et al., 2017; Goncharova & Khaldoyanidi, 2013; Takeshita et al., 2014), which would limit our ability to study the interaction of a limited number of patient derived T-cell subsets with BLECs.

$CD34^+$-derived ECs adhere and grow on nanoporous silicon nitride membranes

Nanoporous silicon nitride (NPN) is a recently developed ultrathin silicon membrane technology (DesOrmeaux et al., 2014). NPN is the third generation of ultrathin porous membrane materials we have developed using silicon manufacturing techniques, following pnc-Si (Striemer et al., 2007) and microporous SiO_2 ($\mu pSiO_2$) (Mazzocchi, Man, DesOrmeaux, & Gaborski, 2014) . These 'nanomembranes' have found broad applications in biomedical sciences including cell culture (Agrawal et al., 2010; Mazzocchi et al., 2014; Nehilla, Nataraj, Gaborski, & McGrath, 2014), lab on chip devices (Carter et al., 2017; Chung et al., 2014) and bioseparations (Johnson et al., 2013; Winans, J. P. Smith, Gaborski, Roussie, & McGrath, 2015). Silicon nanomembranes are ultrathin, optically transparent, biocompatible and highly permeable, which makes them ideal substrates for the construction of *in vitro* barrier models relying on molecular cross-talk with a second cell type Fig. 1A to 1D). The silicon platform also enables ready integration into microfluidic devices (Chung et al., 2014; Johnson et al., 2013).

We considered 400 nm thick microporous $\mu pSiO_2$ (Carter et al., 2017) as a candidate for our human BBB

model, however we have found that human umbilical vein endothelial cells (HUVECs) do not adhere to these membranes in the presence of flow regardless of surface treatments (Supplemental Figure 1). By contrast HUVECs readily adhere, and even align on NPN, in the presence of shear stresses up to 10 dynes/cm^2 applied continuously for 24+ hours (Supplemental Figure 1). Various surface coating techniques were implemented to improve the cell adhesion on the µpSiO_2 substrates. Extracellular matrix (ECM) proteins such as fibronectin, collagen 1, as well as basement membrane mimetic compositions (Geltrex™, Corning, NY) were tested. Aminopropyl triethoxy silane (APTES) - 4% in acetone and 100% - were also used to modify the surface properties to enhance cell adhesion under shear stress. None of the coating methods prevented cell detachment from the microporous substrate under shear stress and the substrate was decellularized in few hours post-flow (data not shown). Thus, we selected NPN as our membrane of choice and confirmed that CD34$^+$-derived ECs efficiently adhered to and built confluent monolayers on Matrigel™-coated NPN with glass-like optical character ideal for *in vitro* live cell imaging (Fig. 1E).

Pericyte co-culture can be replaced by pericyte-conditioned medium to induce BBB characteristics in CD34$^+$-derived ECs

Co-culture of CD34$^+$-derived ECs with pericytes has been shown to be essential for induction of BBB characteristics (Cecchelli et al., 2014). This procedure involves changes in gene expression of Wnt signaling, tight junctions and transporters that occur over 6 days of co-culture (Cecchelli, 2014). In theory, co-culture of ECs and pericytes could be accommodated by designing a two-chamber microfluidic device with the EC grown on the silicon membrane in the upper compartment and the pericytes in the lower compartment. The major disadvantage of this set up would be that *in vitro* live cell imaging of the BBB under flow employs inverted microscopy, which positions the pericyte culture between the microscope objective and the EC monolayer potentially impairing the imaging quality of the EC monolayer. We therefore asked if the pericyte-co-culture could be replaced by administrating the conditioned medium of the pericyte cultures. To this end, we co-cultured CD34$^+$-derived ECs with or without pericytes in the original Transwell® filter co-culture setup for 5 days as positive and negative control, respectively. In parallel CD34$^+$-derived ECs plated on additional matrigel coated Transwell® filter inserts were co-

incubated with pericyte-conditioned medium (PCM) from the abluminal (lower compartment) or luminal (upper compartment) side (Fig. 2A,B) and subsequently replaced on a daily basis by alternating between 24h and 48h In order to obtain the PCM, $2.25x10^4$ /well pericytes were seeded into 24-well Costar plates one day prior to seeding the $CD34^+$-derived ECs. After the adhesion of the $CD34^+$-derived ECs on the Matrigel coated Transwell® filter inserts, the 24 hours PCM was collected from the pericyte cultures and administered to the luminal or abluminal side of the $CD34^+$-derived ECs (Fig. 2A,B) and subsequently replaced on a daily basis by alternating between 24h and 48h PCM to ensure an optimal concentration of the pericyte-derived factors (Fig. 2B). After 5 days of culturing the $CD34^+$-derived ECs under the different conditions, their barrier characteristics were compared side-by-side by testing the permeability of the EC monolayers for the small molecular weight tracer lucifer yellow (LY) (Fig. 2C). In accordance to our previous findings the monoculture of $CD34^+$-derived ECs did not establish a diffusion barrier for LY (Pe LY = $2.04 \pm 0.19 \times 10^{-3}$ cm/min), while the co-culture with pericytes established brain-like endothelial cells (BLECs) with tight barrier characteristics as shown by the significantly reduced clearance of LY across the EC monolayer (Pe LY = $0.52 \pm 0.08 \times 10^{-3}$ cm/min; Fig. 2C). PCM applied from the abluminal side of the $CD34^+$-derived EC monolayer induced barrier characteristics comparable to those induced by the pericyte-coculture (Pe LY = $0,55 \pm 0,06 \times 10^{-3}$ cm/min; Fig. 2C). Interestingly, applying PCM from the luminal side failed to induce comparable barrier characteristics, which underscores that our *in vitro* model of the BBB appropriately mimics the *in vivo* situation with pericytes embedded in the endothelial basement membrane at the abluminal side of the brain microvascular endothelial cells.

Following the permeability assay, the EC monolayers were stained for the transmembrane adherens and tight junction proteins VE-cadherin and claudin-5, respectively and the junctional scaffolding protein ZO-1 to address the junctional integrity and maturation. The staining revealed that PCM when applied from the abluminal side induced a junctional architecture in $CD34^+$-derived ECs comparable to that induced by co-culture with bovine pericytes (Cecchelli et al., 2014). Specifically, the pericyte co-culture or the abluminally administered PCM induced a continuous and more jagged staining of the junctional and scaffolding proteins VE-Cadherin and ZO-1 compared to the monoculture and PCM luminal conditions (Fig. 2D). Moreover, junctional claudin-5 immunostaining was enhanced in BLECs under conditions of pericytes

co-culture and in the abluminally administered PCM conditions (Fig. 2D) when compared to controls. In addition, the F-actin staining revealed absence of stress fibers underscoring the quiescent nature of the ECs monolayers (Fig. 2D). Overall, these results confirmed that $CD34^+$ -derived ECs are polarized and that the barrier-inducing signals provided by the pericytes have to be provided from the abluminal side to induce BBB characteristics like junctional maturation and low permeability to small molecules. Taken together, these results show that differentiation of $CD34^+$-derived ECs into BLECs does not rely on true co-culture with pericytes; it can equally well be achieved by applying PCM to the abluminal side.

$CD34^+$-derived ECs establish BBB characteristics when grown on NPN membranes

In a next step, we asked if PCM induced barrier characteristics in $CD34^+$-derived ECs also occurred when the cells were grown on NPN membranes. For this purpose, we fabricated an open format device, which we referred to as "Transwell mimetic", in which a NPN membrane divides an upper and lower compartment (Fig. 3A). The membrane compartment of this device is open for media and reagent application from the top and promotes easy gas exchange for maintaining physiological pH within the media. The basal compartment can be easily accessed from fluid ports on the top of the device and is separated from the membrane compartment with the NPN membrane providing the sole area for exchange of factors between compartments. The entire device can be autoclaved and the volume requirements in the upper and lower compartments is 50 µL and 20 µL respectively.

In order to induce barrier characteristics in $CD34^+$-derived ECs, we followed the same culture procedure as depicted in Fig. 2B. $CD34^+$-derived ECs ($1x10^5$ cells/mL) were seeded on the Matrigel coated NPN membrane and grown in the absence or presence of PCM applied in the basal compartment (Fig. 3B). $CD34^+$-derived ECs were cultured for 5 days replacing the PCM in the basal compartment every 24 hours alternating the 24h and 48h PCM. Barrier characteristics were tested after 5 days of culture by performing a LY permeability assay (Fig. 3B). The paracellular permeability value across the endothelial monolayers). The paracellular permeability value across the endothelial monolayers was evaluated as described in details in Material & Methods and the PSe was divided by a cell growing area (0,014 cm^2), in order to generate the endothelial Pe in cm/min. The permeability assay revealed that $CD34^+$ - derived ECs grown

on NPN membranes in monocultures did not establish a tight barrier with a permeability coefficients Pe LY = 1.82 ±0.18 x10^{-3} cm/min. In contrast in the presence of abluminal PCM, $CD34^+$ -derived ECs grown on NPN membranes established BLEC characteristics with a permeability coefficient Pe LY= 0.39 ± 0.07 x10^{-3} cm/min (Fig. 3B), which is comparable to the LY paracellular permeability of BLECs grown on Transwell® filter inserts (Fig. 2A). Thus, NPN membranes are suitable for the induction of BBB properties by PCM in $CD34^+$ -derived ECs. BLEC properties were further confirmed by confirming the junctional localization of VE-cadherin, claudin-5 and ZO-1 in BLECs gown on NPN membranes in the presence of abluminal PCM (Fig. 3C).

Next, we investigated cell surface expression of adhesion molecules known to mediate T-cell interaction with the BBB on BLECs grown on the NPN membranes. We found constitutive cell surface expression of the adhesion molecule ICAM-2, constitutively expressed in human endothelial cells (Bo et al., 1996) and to a lesser degree for ICAM-1 but not of VCAM-1 on BLECs (Fig. 3D). To mimic an inflammatory environment, BLECs were stimulated with tumor necrosis factor alpha (TNF-α) activating e.g. the pleiotropic nuclear factor–kB (NF-kB) (Collins et al., 1995). Accordingly, BLECs showed an up-regulation of ICAM-1 and VCAM-1 after stimulation with TNF-α (10 ng/mL) for 16 h. Moreover, the TNF-α stimulation was inducing the formation of F-actin stress fibers as revealed by the immunofluorescence staining (Fig. 3D). Taken together, these results show that our human *in vitro* BBB model is functionally reproduced on our customized silicon nanomembrane system and suitable to investigate the role of the signature molecules involved in the T cell trafficking.

Establishment of a small scale human in vitro BBB model under flow: Introduction of the µSiM-CVB flow system

The physical and optical characteristics of the NPN membranes make it possible to create flow chambers with microliter scale volumes and a robust performance. This allowed for designing a novel small scale two-chamber flow device, which we refer to as "µSiM-CVB flow system" (Fig. 4A). This new device is composed of several 300 µm thick silicone layers that create the compartments necessary for the apical growth of the $CD34^+$ -derived ECs and the abluminal application of PCM. The top of the µSiM-CVB flow

system is sealed by a layer of gas-permeable and transparent PDMS with fluid access ports to both the top and bottom compartments of the device. The $CD34^+$ -derived ECs are seeded on the silicon nanomembrane via the top channel that also serves as the flow channel, while the bottom channel is strictly accessed by pipettes. In addition, the PDMS reservoirs on top of the device at both ends of the 2 channels allow the addition of excess culture medium (200 µL per channel) to prevent evaporation during prolonged cell culture (Fig. 4B). In order to grow the BLECs monolayer, $CD34^+$ -derived ECs are seeded in the top channel on the silicon nanomembrane (1.4 mm^2) at a concentration of $1x10^6$ cells/mL. Then, the induction of BLECs is achieved by the daily and alternating administration of 24h and 48h PCM for 6 days, as established in the "Transwell mimetic" system. To apply flow on the BLEC monolayers, both ends of the top channels are connected with a transparent PVC tubing (Ø = 1 mm) with the help of 18 gauge straight needles. The inlet tubing is then connected to a 3-way tap linked to 2 reservoirs respectively containing the Th1 cell suspension and migration assay medium, and the outlet tubing was connected to a programmable pump that is pulling medium over the BLEC monolayer to create a controlled laminar flow. With this device and scheme, it was possible to superfuse the Th1 cells over the BLECs monolayer and directly image the T cells in phase contrast with a transmitted light inverted microscope (Axio Observer Z1, Zeiss) equipped with a temperature-controlled chamber (37°C), and to observe the multi-step T-cell migration across the BBB under physiological flow in vitro (scheme in Fig. 4C). To perform the flow experiment, first the Th1 cells were infused in the top channel for 4 min at a low flow rate of 0.1 dyne/cm^2 to allow a first contact with the BLECs (accumulation phase). Then the migration assay medium only was infused and the flow rate was increased to 1.5 dyne/cm^2 to reach a physiological shear for 30 min (shear phase). In order to see if we could image the BLECs at high resolution and keep the focus on the cells for the duration of the flow experiment, a temporal snapshot of the BLECs taken from a video recorded with a 10x magnification was made, showing the first and last frame of an area where T cells did not attach to the BLECs monolayer (Fig. 4D). In order to mimic conditions of the BBB under inflammatory or non-inflammatory conditions, BLECs were pre-treated or not with TNF-α after 5 days of culture with the PCM, when the BBB characteristics (permeability, expression of tight junction molecules) were established (Fig. 3B,C), 16h before starting the flow experiment recorded with a 10x objective (EC Plan-Neofluar 10X/0.30

Ph1). First, we found that the resolution was sufficient to perfectly distinguish each endothelial cell in phase contrast images. Then, we could observe that treatment of BLECs with TNF-α induced a more elongated shape of the BLECs (Fig. 4D), which is in accordance with the induction of F-actin stress fibers as observed with the immunofluorescence staining (Fig. 3D). When starting to apply flow (0 min) the NPN membrane's stiffness kept it perfectly in focus (34min55s) and allowed us to continuously image the BLEC monolayer under physiological flow in the same focal plane. In addition, we ensured that the monolayer stayed perfectly intact and in focus under physiological flow for a time period of at least 30 minutes, which is a prerequisite for following the T cell-BLECs interactions over time.

Live cell imaging of the interaction of human T cells with BLECs under physiological flow

In a final step, we employed the μSiM-CVB to study the interaction of human T cells with the human BBB under physiological flow. To infuse T cells on the BLECs monolayer, we aspirated human Th1 cells from a reservoir via an inlet tubing over the BLEC monolayer for 4 minutes with a flow rate of 0.1 dyne/cm^2 (accumulation phase). After this accumulation phase the flow rate was increased to a physiological flow rate of 1.5 dyne/cm^2 for 30 min (shear phase) allowing to study post-arrest T-cell behavior on the BLECs monolayer under physiological flow by live cell imaging.

In order to illustrate how we could observe various types of T cell/BLEC interactions with high resolution, we generated temporal snapshots from a video recorded with a 20x magnification where BLECs were stimulated with TNF-α (Fig. 5A). In addition, we also recorded videos with a 10x magnification of T cell-BLEC interactions where BLECs were stimulated (video 2) or not (video 1) with TNF-α. These 10x magnifications videos allowed us to have a statistical comparison of the T-cell behavior on the BLEC monolayers in unstimulated and TNF-α stimulated conditions (Fig. 5B), since a higher number of T cells could be tracked compared to higher magnification videos, at the cost of a lower resolution. To analyze the respective T-cell behavior on the BLECs monolayers in a quantitative manner, we performed a visual frame-by-frame offline analysis of the time-lapse videos. To this end each T cell was categorized into a specific behavioral group. Under both, unstimulated and TNF-α stimulated conditions, the majority of T cells were found to polarize upon arrest (video 1 and 2) and to migrate across the BLEC monolayer with or

without prior crawling on the BLECs. These were categorized under “diapedesis” (Fig. 5A). T cells that crawled on the surface of the BLECs for the entire observation time were categorized as “crawling” (video 1 and 2, Fig. 5A). One additional behavior observed was T cells that remained stationary without displacing beyond a distance exceeding their own diameter and presenting dynamic cellular protrusions and thus “probing” the BLEC monolayer (video 1 and 2, Fig. 5A). Also, a certain number of T cells were found to quickly “detach” from the BLECs monolayer when the flow rate increased at the beginning of the shear phase (video 2). In general, we observed a higher number of T cells arresting on the TNF-α stimulated BLECs versus the non-stimulated BLECs monolayers resulting in an increased number of T cells interacting with the TNF-α stimulated BLECs in each T cell behavioral category (Fig. 5B). Overall, the TNF-α stimulation favored T cell-BLECs interactions without modulating their behavior among categories. This observation is in accordance with the upregulated cell surface expression of ICAM-1 and VCAM-1 previously shown (Fig. 3D), suggesting that upon TNF-α stimulation, the upregulation of adhesion molecules could explain the significantly higher number of Th1 cells found to arrest on BLECs under physiological flow, ~4 min after starting to infuse T cells and just after the accumulation phase (Fig. 5B). Taken together, our novel µSiM-CVB flow system allows for detailed observation of the multi-step T cell extravasation across a human model of the BBB at a very small scale suitable for employing rare patient derived immune cells.

Discussion

The development of an *in vitro* platform to study the migration of immune cells across the BBB in the context of disorders of the human CNS presents several challenges. We have recently faced this challenge by establishing a novel human *in vitro* model of the BBB from human ECs derived from cord blood CD34+ hematopoietic stem cells (Cecchelli et al., 2014). We demonstrated that when co-cultured with pericytes, $CD34^+$ EC differentiate into brain-like endothelial cells (BLECs) establishing low permeability barriers and mature tight junctions. Due to the general availability of cord blood stem cells, BLECs can be widely adopted to study molecular mechanisms in pathologies implicating the BBB such as neurodegenerative or

neuroinflammatory disorders (e.g. Alzheimer's disease, multiple sclerosis), stroke and traumatic brain injury, infectious processes and inflammatory pain.

While we have previously used BLECs to study immune cell extravasation across the BBB in static culture conditions (Lyck et al., 2017), the application of physiological flow is needed for more physiological observations. Physiological flow has been shown to have a significant impact on T-cell diapedesis across vascular monolayers *in vitro* (Schreiber et al., 2007; Steiner et al., 2011). The visualization of the multi-step immune cell extravasation across the vascular wall requires a testing platform compatible with transmitted light microscopy, preferably phase contrast. The desire for flow and live-cell imaging has compelled us and others to use flow chambers with endothelial cells cultured on glass coverslips, as the track-etched membranes used in traditional two-chamber filter devices are notoriously bad for imaging under transmitted light (Carter et al., 2017). This choice however, introduces new complications as non-permeable substrates are not physiological and are thought to compromise the polarization of barrier cells due to the lack of basal transport (Samuel et al., 2017). In addition, these flow chambers are not suitable for *in vitro* BBB models that rely on the continuous and polarized cross-talk of the brain endothelial cells with cellular elements of the neurovascular unit, such as pericytes or astrocytes (Engelhardt & Liebner, 2014; Hawkins & Davis, 2005). Here, we provide new and compelling evidence of the need for a dual compartment for maintaining barrier characteristics in our human *in vitro* BBB model: the addition of pericyte conditioned media (PCM) to the basal, but not to the apical compartment, was sufficient for the induction of tight BLEC barriers (Fig. 2A). Thus, $CD34^+$ ECs monocultures on non-permeable glass or tissue culture plastic would not mimic the human BBB *in vitro*, even in conditioned media.

Our experiences identify a minimum set of device requirements for the study of immune cell migration across the BBB under physiological flow by live cell imaging; the device must: 1) be transparent, 2) enable physiological flow in the luminal compartment, and 3) include a permeable yet sufficiently stiff cell-substrate so that flow doesn't shift the image focus. The previous decade has witnessed the emergence of customized microsystems for 'organ-on-chip' models or 'microphysiological systems' (MPS) (Bhatia &

Ingber, 2014). While a number of these efforts have focused on BBB (Cucullo et al., 2008; Goncharova & Khaldoyanidi, 2013; Herland et al., 2016; Takeshita et al., 2014; Xu et al., 2016), only Walter and colleagues (Walter et al., 2016) addressed the need for membrane transparency. Their solution was to employ 'transparent' track etched membranes that have 100 fold fewer pores than conventional materials (10^6 pores/cm^2 vs 10^8 pores/cm^2) and are more than twice as thick (23 µm vs 6 – 10 µm). While these membrane modifications diminish the confounding influence of pores on light transmission and enabled the team to acquire clear phase images of monolayers, they also dramatically reduce the diffusive permeability of the membranes by more than two orders of magnitude. Indeed, we calculated the small molecule permeability of the low porosity TE membranes used by Walter et al. to be 10^{-5} cm/s, a value lower than some of the permeabilities we report here for luciferase yellow transport across BLEC monolayers. Thus, these low porosity TE membranes can be rate limiting for small molecule transport if used in a two chambers system. This would mask the properties of monolayers in barrier measurements and may prohibit induction of BBB characteristics in endothelial monolayers grown on these membranes because of the hindrance of small molecule diffusion to and from the basal side of cells.

We addressed the need for optical transparency by building the first in vitro BBB model that features silicon nanomembrane technology. Silicon nanomembranes are free-standing porous membranes produced by silicon microfabrication methods and with a thickness that can be tuned between 15 nm (Striemer et al., 2007) and 400 nm (de Mesy Bentley et al., 2017). The nanomembranes used for the novel flow chamber device were 50 nm thick nanoporous silicon nitride (NPN) (DesOrmeaux et al., 2014) with ~ 50 nm pores and a density of 10^{11} pores/cm^2. The small molecule diffusive permeability of these membranes is a remarkable ~ 0.1 cm/s (Kim et al., 2008), a value so high that is indistinguishable from free diffusion through water in practical assays (Snyder et al., 2011). In other words, small molecule diffusion across a nanomembrane occurs as if the membrane is not there, even as it provides a physical divide to define the compartments of a two-chamber system.

The superior imaging characteristics of nanomembranes have been appreciated in cell culture studies for

some time (Agrawal et al., 2010; Carter et al., 2017), but they have never been used for live cell imaging or functional BBB studies before now. The microporous SiO_2 membranes employed by Carter et al. for example, do not support adhesion under physiological flow (Figure S1). Here we show the compatibility of NPN with the growth of human BLECs monolayers and the adhesion of these monolayers under physiological flow. Thus, because of its physical properties combining high permeability with thinness and stiffness as well as its better biocompatible characteristic under flow, we chose the NPN membrane over the SiO_2 membrane to build our μSiM-CVB flow system. The elimination of the need for maintaining barrier characteristics in BLECs by co-culture with pericytes through the use of pericyte-conditioned media in the basal compartment, is another key innovation. The introduction of two cell types to microculture devices is technically challenging, as is distinguishing between these cell types across a nanomembrane that is thinner than the diffraction limit of light (Carter et al., 2017). With pericyte conditioned media in the basal compartment of closed microdevices equipped for flow in the apical compartment, we were able to maintain BBB characteristics in BLECs while ensuring the visibility of the monolayer as a prerequisite to study of T-cell migration across the BBB under flow. The requirement of membrane stiffness comes about because we have seen polymer membranes deflect with the onset of flow resulting in a change of focus during live imaging. Despite their high porosity and extreme thinness, the high Young's modulus of silicon nitride helps NPN membranes resist deflection with small pressure changes, particularly at the membrane dimensions (2 mm x 0.7 mm) that we use here (Gillmer et al., 2017).

The uniqueness of the microsystem presented in this study extends beyond superior imaging quality, and features ease of assembly and use, the potential for high throughput manufacturing, and importantly, operation with microfluidic volumes. The volumes of the basal channels in both the "Transwell mimetic" and the μSiM-CVB flow system, and the apical channel in the μSiM-CVB flow system of the device are less than 20 μL. This feature will eventually allow the use of small samples of body fluids or cells obtained from patients for personalized medicine. Even for *in vitro* mouse models, microfluidic volumes of these devices are beneficial, since the volume of body fluids of mice are equally small. For example, a metabolic profile analysis is difficult to achieve unless the working sample volumes are on the same order as the volumes in

the body.

In our present study, NPN membranes were superior to any commercially available membrane systems with respect to their optical characteristics and most critically by providing the adhesive properties that allowed maintenance of a BLEC monolayer under physiological flow. Indeed, the $CD34^+$ ECs grew perfectly on the NPN membrane reaching confluency 24h after seeding and building a dense monolayer after 6 days of culture. Because the silicon platform enables the facile construction of dual compartment culture devices, we readily adapted the co-culture based human *in vitro* BBB model requiring co-culture of $CD34^+$ ECs with pericytes (Cecchelli et al., 2014). Successfull replacement of the pericyte co-culture with pericyte-conditioned medium (PCM) supplied from the basal compartment further advanced the human *in vitro* BBB model for in vitro live cell imaging. Basal application of PCM allowed for differentiation the $CD34^+$ ECs in BLECs monolayers with low permeability to small molecular tracers and BBB like morphology as visualized by the junctional localization of VE-cadherin, claudin-5 and ZO-1 and the establishment of a cortical Factin ring.

The next step, which was to apply flow in our µSiM-CVB flow system, took full advantage of the properties of the NPN material that help distinguish it from all commercial membrane materials. While its thinness gives it a superior transparency and makes it excellent for live cell imaging, the material is sufficiently stiff that it remains in focus with the onset of flow. Indeed, in our present study we found that applying shear forces up to 1.5 dynes/cm^2 in the apical compartment of our novel device did lose focus in more than 30 minutes of continuous recording. Optical imaging quality of the T-cell interactions observed on the BLECs monolayer using the novel µSiM-CVB flow system were indistinguishable from those previously recorded when studying T cell interaction with endothelial monolayers grown on glass (Rudolph et al., 2016; Shulman et al., 2009; Steiner et al., 2010). The observations of T-cell arrest, crawling on, and diapedesis across the BLECs monolayers under physiological flow as well as the observed influence of the inflammatory status of the BLEC on these interactions, validates the suitability of this novel microfluidic device to serve as an in vitro BBB platform. Furthermore, the small size of the µSiM-CVB flow system

opens the opportunity to investigate rare samples with a limited number of immune cells concentrated in a small volume thanks to the apical channel of 20 µL. The minimum number of immune cells that can be used depends of the proportion of cells that interact with the BLECs and can be imaged in a field of view under the microscope. Determining this number for particular samples will enable multiplex investigations of the interaction of rare disease immune cells isolated from patients with neuroinflammatory disorders (e.g. multiple sclerosis) with the BBB under physiological flow *in vitro*.

Taken together the adaptation of our previously established stem cell derived *in vitro* model of the human BBB to a novel micro-scale nanomembrane based microfluidic device, with superior physical and optical characteristics, provides a powerful tool to study the interaction of a variation of patient derived cells, ranging from immune cells to cancer cells with the human BBB under physiological flow *in vitro.* Overall, we expect this platform to open new opportunities to define novel therapeutic targets for neurological disorders ranging from neuroinflammation to tumor metastasis and for adaptation to investigate other cellular barriers.

Materials and Methods

Device Fabrication

The key feature of the engineered devices used in the cell culture applications presented here is the nanoporous silicon nitride (NPN) membranes, also referred to as silicon nanomembranes. The details of the fabrication of these membranes are provided elsewhere (DesOrmeaux et al., 2014), and are commercially available at SiMPore Inc., Rochester, NY. These membranes are manufactured on 300 micron silicon substrates with a resulting freestanding permeable film that is 50 nm thick with a pore aspect ratio of 1:1 (i.e., average pore diameter is also 50 nm). The overall dimension of the silicon membrane 'chips' is 5.4 x 5.4 mm^2. The permeable area or membrane 'window' of the chip is 2 mm x 0.7 mm.

The microfluidic device used for static and dynamic assays consist of 2 compartments: apical and basal, separated by the permeable membrane chip in between. The apical and basal fluidic compartments or

channels are composed of transparent silicone gaskets (300 microns thick) commercially available from Specialty Silicone Fabricators, CA. The different layers of the devices are shown in Figures 3 and 4 representing the devices for static and flow configurations respectively. The channels and the silicon chip are covalently bonded to each other via surface functionalization of the silicon atoms in each layer. Briefly, both the bonding surfaces are exposed to UV-Ozone environment for 10-15 minutes, followed by thermal curing at 70°C for 2 hours. The fluidic access ports for these devices are provided by a thick slab of poly dimethysiloxane (PDMS) (Sylgard 184, Dow Corning). Flow devices have 4 access ports: 2 for the apical chamber and 2 for the basal chamber, while "Transwell mimetics" only have access ports for the basal chamber. These ports are made by simply punching holes in the PDMS block using a 18 gauge needle. Media reservoirs are added to support cell culture in both types of devices. In the "Transwell mimetic" this is a single reservoir immediate above the membrane while the flow devices have a media reservoir on the top of all the 4 access ports. The reservoirs are made out of PDMS blocks as well with wider punched holes, and bonded to the intermediate PDMS blocks via UV-Ozone exposure. The PDMS blocks and the bottom glass substrates are also bonded to the gaskets-chip-gaskets' assembly using similar UV-Ozone chemistry.

Cell-membrane adhesion assays

Adhesion of endothelial cells was investigated using human umbilical vein endothelial cells (HUVECs). Primary HUVECs were cultured in MCDB-131 complex medium with 10% serum, both purchased from Vec Technologies (Rensselaer, NY), in the presence of 5% CO_2 and 80% humidity at 37 °C. Upon confluence, HUVECs were harvested and introduced in the flow devices consisting of either NPN or microporous silicon dioxide ($\mu pSiO_2$). Prior to cell seeding, the membranes are coated with human plasma fibronectin (Sigma-Aldrich) at ~2 $\mu g/cm^2$ density at room temperature for one hour. Cells were allowed to grow under static conditions for 24 hours, and afterwards were connected to a flow circuit to recirculate media in the cell chamber. Media flow was optimized to yield 10 $dynes/cm^2$ of shear stress on the endothelial cells to mimic physiological levels of veins. Cells were inspected during regular intervals to ensure the adherence of cells on the underlying substrate. Phase contrast images were recorded at 10x magnification using a

Nikon microscope, before the introduction of flow, and after 2 hours and 24 hours. Images of cells adhering on both nanoporous and microporous substrates at relevant time points are as shown in the Supplementary Figure 1.

Isolation and differentiation of $CD34^+$ cells from human umbilical cord blood

The isolation of $CD34^+$ cells required the collection of human umbilical cord blood (UCB) from infants. Parents signed an informed consent form in compliance with French legislation. The protocol was approved by the French Ministry of Higher Education and Research (CODECOH Number DC2011-1321) and all experiments were carried out in accordance with the approved protocol. $CD34^+$ cells were isolated from human umbilical cord blood (UCB) according to a protocol previously reported (Pedroso et al., 2011). Then, $CD34^+$ cells isolated from the UCB were differentiated in ECM basal medium (ScienCell) supplemented with 20% (v/v) fetal bovine serum (FBS; Life Technologies) and 50 ng/mL of $VEGF_{165}$ (PeproTech Inc.), on 1% (w/v) gelatin-coated 24 well plates ($2x10^5$ cells/well). After 15-20 days ECs are seen in the culture dish. For each experiment, the cells were expanded in 0.2% (w/v) gelatin-coated 100 mm Petri dishes (Corning) in ECM basal medium supplemented with 5% FBS, 1% endothelial cell growth supplement (ECGS; ScienCell) and 50 µg/mL gentamycin (Biochrom AG).

Induction of BBB characteristic in $CD34^+$ -derived endothelial cells

Induction of BBB like characteristics in $CD34^+$ -derived endothelial cells was achieved by co-culture with bovine pericytes as described before (Cecchelli et al., 2014). In brief, pericytes were initially seeded on 100-mm gelatin-coated petri dishes (Corning) and cultured in Dulbecco's Modified Eagle's Medium (DMEM) (Life Technologies) supplemented with 20% (v/v) FBS (Life Technologies), 2 mM L- glutamine, 50 mg/mL gentamycin. Upon reaching confluency pericytes ($2.25x10^4$ /well) were seeded into 24-well plates (Costar). On the following day, $CD34^+$-derived ECs grown on gelatin-coated 100 mm petri dishes in ECM (Sciencell) were trypsinized and seeded ($4x10^4$/filter insert) onto Matrigel-coated (Corning, 354230) Transwell® filter inserts (Costar cat n.3495) and placed above the pericyte cultures. At the end of this

culture procedures the $CD34^+$-derived ECs will acquire the features of brain like endothelial cells (BLECs) as revealed by the expression of BBB marker and functional properties revealed by LY permeability assay evaluated from 2 to 20 days of co-culture (Cecchelli et al., 2014).

Endothelial Permeability (Pe) Measurements

Endothelial permeability was investigated by measuring the clearance of Lucifer yellow (LY; 20 nM; Life technologies) across the BLECs monolayer exactly as described before (Cecchelli et al., 2014; Cecchelli et al., 1999; Coisne et al., 2005; Steiner et al., 2010). In brief, prior to experiments, LY (MW 457.3 g/mol) was diluted in assay medium (DMEM (Gibco, Paisley, UK), 5 % FCS (Gibco, Paisley, UK), 25 mM Hepes (Gibco, Paisley, UK), 2 % l-glutamine Gibco, Paisley, UK) as previously published in (Cecchelli et al., 2014) and 100 µl of the LY solution (20 nM) was added to the upper side of the filter inserts, which were subsequently placed into wells containing 600 µl of assay medium. The plate was incubated at 37 °C and the inserts were transferred into wells containing fresh assay medium every 10 min, avoiding long exposure to light and room temperature. 200 µl samples from all lower compartments were transferred to a 96-well plate. For the "Transwell mimetic" system, the membrane compartment was filled with 50 µL of a LY solution (20 nM), and in the basal compartment with 20 µL of permeability assay medium. After 60 min incubation, the assay medium was collected from the basal compartment and the fluorescence was evaluated with the TECAN reader infinite M1000 PRO. A standard dilution curve (20–0.05 µM) and empty filters or "Transwell mimetic" were used to obtain the reference permeability of the empty filter inserts. The permeability coefficient was calculated as follows: the slope of the average tracer volume cleared was plotted versus time in order to obtain the linear regression designated as PSt. The slope of the tracer clearance curve of the coated empty filters was indicated as PSf. The permeability surface area product of the endothelial cell monolayer (PSe) was calculated from PSt and PSf: $1/PSe = 1/PSt - 1/PSf$. The PSe was divided by the filter surface area, in order to generate the epithelial Pe in cm/min. The fluorescence detection was performed using the Tecan Infinite M1000 device and the Tecan i-control software (Tecan Trading AG, Männerdorf, Switzerland).

Stimulation of BLECs with the pro-inflammatory cytokine TNFα

To mimic neuroinflammatory conditions, human brain like endothelial cells (BLECs) were stimulated with human recombinant tumor necrosis factor-α (TNF-α, 210-TA, R&D Systems, Inc.) at a concentration of 10 ng/ml for 16 to 20h prior to performing experiments.

Immunofluorescence stainings of BLECs

For staining in the Transwell® filter inserts, BLECs were fixed in 1% (w/v) formaldehyde diluted in calcium and magnesium-free phosphate- buffered saline (PBS) for 10 min at room temperature (RT) and permeabilized with Triton X-100 (0.1% (w/v) in PBS for 10min at RT. After three rinses with PBS, the filter membranes were carefully cut out with a scalpel and blocked for 30 min with skimmed milk 5% (w/v) in PBS. BLEC monolayers were incubated for 1h at RT with primary antibody against zonula occludens-1 at 5 µg/mL (ZO-1, Thermo Fisher Scientific, 617300) or VE-Cadherin at 7.5 µg/mL (ref. sc-9989; Santa Cruz). For the staining of claudin-5, BLECs were fixed in methanol at -20°C for 30s before a permeabilization step of 20 min at RT in Triton X-100 0.3% in PBS, followed by a blocking step of 20 min at RT in in skimmed milk 5% in PBS. Next BLECs were incubated with primary antibody against claudin-5 at 2.5 µg/mL (Invitrogen, 381700) diluted in skimmed milk 5% (w/v) in PBS. After three washes in PBS cells were incubated with secondary antibody for 30 min at RT with goat anti rabbit/Alexa fluor 488 at 5 µg/mL (life technologies, 11034) for ZO-1 and claudin-5 and goat anti mouse-Cy3 at 7.5 µg/mL (Jackson ImmunoResearch, 115-166-06) for VE-Cadherin. After Triton permeabilization, staining of F-actin was obtained with rhodamine-labeled phalloidin (Invitrogen, R415) 1:50 in PBS for 1h at RT. Nuclei were stained using DAPI at 1 µg/mL. Each filter was mounted on a glass slide under a rounded coverslip, using a drop of Mowiol (Sigma-Aldrich) containing 1,4-diazabicyclo [2.2.2] octane (Sigma-Aldrich) as an antiquenching agent.

For BLECs staining on NPN membranes live cells were incubated with 10 µg/ml of anti-ICAM-1 (R&D system), ICAM-2 (Fitzgerald), or VCAM-1 (Clone 51-10C9, cat 551146) antibody for 20 min at 37°C in the culture medium. After a washing step with PBS, BLECs were fixed with 1% PFA in PBS and permeabilized with Triton X-100 (0.1% (w/v) in PBS for 10min at RT. For ICAM-1 and ICAM-2 staining, cells were incubated with the secondary antibody donkey anti-mouse-Cy3 (Jackson ImmunoResearch, 715-165-151). For F-Actin staining,

after Triton permeabilization, cells were incubated with rhodamine- labeled phalloidin (Invitrogen, R415) 1:50 in PBS for 1h at RT. Nuclei were stained with DAPI at 1 µg/mL. For the staining of ZO-1 and VE-Cadherin, after incubation with primary antibody, BLECs were washed in PBS and incubated with secondary antibodies, goat anti-rabbit-Alexa fluor 488 and goat anti mouse-Alexa fluor 488, respectively, for 30 min at RT. For the claudin-5 staining, the same protocol as for BLECs staining on Transwell® filters was applied. Stainings were analyzed with a fluorescence microscope (Axio Observer, Zeiss) and pictures were acquired at the day of the staining and processed with the ZEN software.

Human peripheral blood T cells

Human $CD4^{+}CD45RO^{+}$ T helper 1 (Th1) cells were obtained by fluorescence activated cell sorting from the peripheral blood of healthy donors according to their specific expression pattern of chemokine receptors ($CXCR3^{+}$, $CCR4^{neg}$ $CCR6^{neg}$) exactly as previously described (Engen et al., 2014; Sallusto et al., 1998). Th1 cells were cultured in the presence of interleukin -2 (IL-2, 500U/ml) for a total of 20 days. At the day of the experiment dead cells were removed by a Ficoll gradient (780g, 20 min, 20°C) and Th1 cells were resuspended in migration assay medium (DMEM w/o phenol red, Hepes 25mM, Foetal Bovine Serum 5%, L-glutamine 4mM) at $1x10^{6}$ cells/mL.

In vitro live cell imaging

BLECs were grown to confluency in ECM basal medium supplemented with 5% FBS, 1% endothelial cell growth supplement (ECGS; ScienCell) and 50 µg/mL gentamycin (Biochrom AG) for 6 days as described before and stimulated or not 16 h to 20 h prior to the assay with TNF-α at 10 ng/mL (R&D System, 210-TA). The flow experiment settings consisted of an open reservoir containing migration assay medium only and another one containing the T cell suspension both connected with an inlet transparent PVC tubing (Ø = 1 mm, Semadeni, ref 1336) to the flow chamber by a 3-way tap allowing to alternatively infuse T cells or migration assay medium without stopping nor disturbing the laminar flow. The inlet and outlet tubing were connected to the flow chamber with an 18 gauge straight needle with the tap open to avoid any increased pressure in the chamber. Flow was applied by connecting the outlet tubing to a syringe

automatically drawn up by a precision pump (Harvard Apparatus, Holliston, MA, USA). The flow rate was calculated as described in (Coisne et al., 2013). Briefly, the shear stress was calculated according to the formula: $\tau = (3 \times \mu \times Q)/(2 \times a^2 \times b)$ with τ = shear stress (dyne/cm^2), μ (coefficient of viscosity) = 0.0083 dyne x sec/cm^2 (migration assay medium), Q (volumetric flow rate) = variable controlled by the pump in cm^3/sec, a (half height of the chamber) = 0.015 cm, b (width of chamber) = 0.2 cm. To allow for the accumulation of sufficient Th1 cells on the BLECs monolayer, Th1 cells were first infused with a flow rate of 0.1 dyne/cm^2 for 4 min (accumulation phase). After the accumulation phase, the tap is switched to infuse migration assay medium only and the flow rate was increased to 1.5 dyne/cm^2 thus mimicking a physiological laminar flow condition for 30 min (shear phase). T-cell interaction with the BLECs was recorded for 30 min in time lapse mode (1 picture/5 s) with 10x (EC Plan-Neofluar 10X/0.30 Ph1) or 20x (LD Plan-Neofluar 20X/0.4 Korr Ph2) objectives with a field of view (FOV) respectively of 0.645 µm x 0.645 µm and 0.323 µm x 0.323 µm using an inverted research microscope (Axio observer Z1, Zeiss) equipped with a camera (Zeiss Axiocam MRm) and the ZEN-blue software. The microscopic equipment used for the *in vitro* live cell imaging has been described in depth before (Coisne et al., 2013). Video editing was performed with the software "Adobe After Effect" allowing to export the image sequences as videos running at 30 frames/s as well as to edit the videos to show the different T cell behavior with the BLECs. Fiji software was used to classify the T cell behavioral categories observed on the BLECs under physiological flow (diapedesis, crawling, probing and detaching).

Statistical analysis

Data are shown as the mean ± SEM. Statistical significance was assessed by Student's t-test or one- way ANOVA followed by Dunett's post hoc test. For multiple comparison p-values are indicated in the corresponding figures (**** $p < 0.0001$). Statistical analyses comprising calculation of degrees of freedom were done using GraphPad Prism 6 software (Graphpad software, La Jolla, CA, USA).

Acknowledgements

We gratefully acknowledge Thomas Andolsek for the initial phase of device manufacturing and the support of the Microscopy Imaging Center of the University of Bern.

Funding

This study was funded by the Swiss National Science Foundation (CRSII3_154483, Sinergia UnmetMS) to BE and FS, the Swiss Multiple Sclerosis Society to AM and the Germaine de Stael PHC program to FG and BE. JLM and TK were supported by NIH R01 HL125265.

Competing interests

J.L.M. declares a competing financial interest as a co-founder and equity holder of SiMPore Inc., a commercial manufacturer of NPN and other silicon-based membrane materials.

References

Abadier, M., Haghayegh Jahromi, N., Cardoso Alves, L., Boscacci, R., Vestweber, D., Barnum, S., . . . Lyck, R. (2015). Cell surface levels of endothelial ICAM-1 influence the transcellular or paracellular T-cell diapedesis across the blood-brain barrier. *Eur J Immunol, 45*(4), 1043-1058. doi:10.1002/eji.201445125

Abbott, N. J., Patabendige, A. A., Dolman, D. E., Yusof, S. R., & Begley, D. J. (2010). Structure and function of the blood-brain barrier. *Neurobiol Dis, 37*(1), 13-25. doi:10.1016/j.nbd.2009.07.030

Agrawal, A. A., Nehilla, B. J., Reisig, K. V., Gaborski, T. R., Fang, D. Z., Striemer, C. C., . . . McGrath, J. L. (2010). Porous nanocrystalline silicon membranes as highly permeable and molecularly thin substrates for cell culture. *Biomaterials, 31*(20), 5408-5417. doi:10.1016/j.biomaterials.2010.03.041

Bhatia, S. N., & Ingber, D. E. (2014). Microfluidic organs-on-chips. *Nat Biotechnol, 32*(8), 760-772. doi:10.1038/nbt.2989

Bo, L., Peterson, J. W., Mork, S., Hoffman, P. A., Gallatin, W. M., Ransohoff, R. M., & Trapp, B. D. (1996). Distribution of immunoglobulin superfamily members ICAM-1, -2, -3, and the beta 2 integrin LFA-1 in multiple sclerosis lesions. *J Neuropathol Exp Neurol, 55*(10), 1060-1072.

Canfield, S. G., Stebbins, M. J., Morales, B. S., Asai, S. W., Vatine, G. D., Svendsen, C. N., . . . Shusta, E. V. (2017). An isogenic blood-brain barrier model comprising brain endothelial cells, astrocytes, and neurons derived from human induced pluripotent stem cells. *J Neurochem, 140*(6), 874-888. doi:10.1111/jnc.13923

Carman, C. V., Sage, P. T., Sciuto, T. E., de la Fuente, M. A., Geha, R. S., Ochs, H. D., . . . Springer, T. A. (2007). Transcellular diapedesis is initiated by invasive podosomes. *Immunity, 26*(6), 784-797. doi:10.1016/j.immuni.2007.04.015

Carter, R. N., Casillo, S. M., Mazzocchi, A. R., DesOrmeaux, J. S., Roussie, J. A., & Gaborski, T. R. (2017). Ultrathin transparent membranes for cellular barrier and co-culture models. *Biofabrication, 9*(1), 015019. doi:10.1088/1758-5090/aa5ba7

Cayrol, R., Haqqani, A. S., Ifergan, I., Dodelet-Devillers, A., & Prat, A. (2011). Isolation of human brain endothelial cells and characterization of lipid raft-associated proteins by mass spectroscopy. *Methods Mol Biol, 686*, 275-295. doi:10.1007/978-1-60761-938-3_13

Cecchelli, R., Aday, S., Sevin, E., Almeida, C., Culot, M., Dehouck, L., . . . Ferreira, L. (2014). A stable and reproducible human blood-brain barrier model derived from hematopoietic stem cells. *PLoS One, 9*(6), e99733. doi:10.1371/journal.pone.0099733

Cecchelli, R., Dehouck, B., Descamps, L., Fenart, L., Buee-Scherrer, V. V., Duhem, C., . . . Dehouck, M. P. (1999). In vitro model for evaluating drug transport across the blood-brain barrier. *Adv Drug Deliv Rev, 36*(2-3), 165-178.

Chung, H. H., Chan, C. K., Khire, T. S., Marsh, G. A., Clark, A., Jr., Waugh, R. E., & McGrath, J. L. (2014). Highly permeable silicon membranes for shear free chemotaxis and rapid cell labeling. *Lab Chip, 14*(14), 2456-2468. doi:10.1039/c4lc00326h

Cinamon, G., Grabovsky, V., Winter, E., Franitza, S., Feigelson, S., Shamri, R., . . . Alon, R. (2001). Novel chemokine functions in lymphocyte migration through vascular endothelium under shear flow. *J Leukoc Biol, 69*(6), 860-866.

Cinamon, G., Shinder, V., & Alon, R. (2001). Shear forces promote lymphocyte migration across vascular endothelium bearing apical chemokines. *Nat Immunol, 2*(6), 515-522. doi:10.1038/88710

Coisne, C., Dehouck, L., Faveeuw, C., Delplace, Y., Miller, F., Landry, C., . . . Dehouck, B. (2005). Mouse syngenic in vitro blood-brain barrier model: a new tool to examine inflammatory

events in cerebral endothelium. *Lab Invest, 85*(6), 734-746. doi:10.1038/labinvest.3700281

Coisne, C., Lyck, R., & Engelhardt, B. (2013). Live cell imaging techniques to study T cell trafficking across the blood-brain barrier in vitro and in vivo. *Fluids Barriers CNS, 10*(1), 7. doi:10.1186/2045-8118-10-7

Collins, T., Read, M. A., Neish, A. S., Whitley, M. Z., Thanos, D., & Maniatis, T. (1995). Transcriptional regulation of endothelial cell adhesion molecules: NF-kappa B and cytokine-inducible enhancers. *Faseb j, 9*(10), 899-909.

Cucullo, L., Couraud, P. O., Weksler, B., Romero, I. A., Hossain, M., Rapp, E., & Janigro, D. (2008). Immortalized human brain endothelial cells and flow-based vascular modeling: a marriage of convenience for rational neurovascular studies. *J Cereb Blood Flow Metab, 28*(2), 312-328. doi:10.1038/sj.jcbfm.9600525

de Mesy Bentley, K. L., Trombetta, R., Nishitani, K., Bello-Irizarry, S. N., Ninomiya, M., Zhang, L., . . . Schwarz, E. M. (2017). Evidence of Staphylococcus Aureus Deformation, Proliferation, and Migration in Canaliculi of Live Cortical Bone in Murine Models of Osteomyelitis. *J Bone Miner Res, 32*(5), 985-990. doi:10.1002/jbmr.3055

Deli, M. A., Abraham, C. S., Kataoka, Y., & Niwa, M. (2005). Permeability studies on in vitro blood-brain barrier models: physiology, pathology, and pharmacology. *Cell Mol Neurobiol, 25*(1), 59-127.

DesOrmeaux, J. P., Winans, J. D., Wayson, S. E., Gaborski, T. R., Khire, T. S., Striemer, C. C., & McGrath, J. L. (2014). Nanoporous silicon nitride membranes fabricated from porous nanocrystalline silicon templates. *Nanoscale, 6*(18), 10798-10805. doi:10.1039/c4nr03070b

Diebold, M., & Derfuss, T. (2016). Immunological treatment of multiple sclerosis. *Semin Hematol, 53 Suppl 1*, S54-57. doi:10.1053/j.seminhematol.2016.04.016

Eigenmann, D. E., Xue, G., Kim, K. S., Moses, A. V., Hamburger, M., & Oufir, M. (2013). Comparative study of four immortalized human brain capillary endothelial cell lines, hCMEC/D3, hBMEC, TY10, and BB19, and optimization of culture conditions, for an in vitro blood-brain barrier model for drug permeability studies. *Fluids Barriers CNS, 10*(1), 33. doi:10.1186/2045-8118-10-33

Engelhardt, B., & Liebner, S. (2014). Novel insights into the development and maintenance of the blood-brain barrier. *Cell Tissue Res, 355*(3), 687-699. doi:10.1007/s00441-014-1811-2

Engelhardt, B., & Ransohoff, R. M. (2012). Capture, crawl, cross: the T cell code to breach the blood-brain barriers. *Trends Immunol, 33*(12), 579-589. doi:10.1016/j.it.2012.07.004

Engen, S. A., Valen Rukke, H., Becattini, S., Jarrossay, D., Blix, I. J., Petersen, F. C., . . . Schenck, K. (2014). The oral commensal Streptococcus mitis shows a mixed memory Th cell signature that is similar to and cross-reactive with Streptococcus pneumoniae. *PLoS One, 9*(8), e104306. doi:10.1371/journal.pone.0104306

Enzmann, G., Mysiorek, C., Gorina, R., Cheng, Y. J., Ghavampour, S., Hannocks, M. J., . . . Sorokin, L. (2013). The neurovascular unit as a selective barrier to polymorphonuclear granulocyte (PMN) infiltration into the brain after ischemic injury. *Acta Neuropathol, 125*(3), 395-412. doi:10.1007/s00401-012-1076-3

Erbeldinger, N., Rapp, F., Ktitareva, S., Wendel, P., Bothe, A. S., Dettmering, T., . . . Fournier, C. (2017). Measuring Leukocyte Adhesion to (Primary) Endothelial Cells after Photon and Charged Particle Exposure with a Dedicated Laminar Flow Chamber. *Front Immunol, 8*, 627. doi:10.3389/fimmu.2017.00627

Garberg, P., Ball, M., Borg, N., Cecchelli, R., Fenart, L., Hurst, R. D., . . . Osterberg, T. (2005). In vitro models for the blood-brain barrier. *Toxicol In Vitro, 19*(3), 299-334. doi:10.1016/j.tiv.2004.06.011

Gillmer, S. R., Fang, D. Z., Wayson, S. E., Winans, J. D., Abdolrahim, N., DesOrmeaux, J.-P. S., . . . McGrath, J. L. (2017). Predicting the failure of ultrathin porous membranes in bulge tests. *Thin Solid Films, 631*, 152-160. doi:https://doi.org/10.1016/j.tsf.2017.04.004

Goncharova, V., & Khaldoyanidi, S. K. (2013). A novel three-dimensional flow chamber device to study chemokine-directed extravasation of cells circulating under physiological flow conditions. *J Vis Exp*(77), e50959. doi:10.3791/50959

Grant, G. A., Abbott, N. J., & Janigro, D. (1998). Understanding the Physiology of the Blood-Brain Barrier: In Vitro Models. *News Physiol Sci, 13*, 287-293.

Hawkins, B. T., & Davis, T. P. (2005). The blood-brain barrier/neurovascular unit in health and disease. *Pharmacol Rev, 57*(2), 173-185. doi:10.1124/pr.57.2.4

Helms, H. C., Abbott, N. J., Burek, M., Cecchelli, R., Couraud, P. O., Deli, M. A., . . . Brodin, B. (2016). In vitro models of the blood-brain barrier: An overview of commonly used brain endothelial cell culture models and guidelines for their use. *J Cereb Blood Flow Metab, 36*(5), 862-890. doi:10.1177/0271678x16630991

Herland, A., van der Meer, A. D., FitzGerald, E. A., Park, T. E., Sleeboom, J. J., & Ingber, D. E. (2016). Distinct Contributions of Astrocytes and Pericytes to Neuroinflammation Identified in a 3D Human Blood-Brain Barrier on a Chip. *PLoS One, 11*(3), e0150360. doi:10.1371/journal.pone.0150360

Johnson, L. M., Gao, L., Shields, I. C., Smith, M., Efimenko, K., Cushing, K., . . . Lopez, G. P. (2013). Elastomeric microparticles for acoustic mediated bioseparations. *J Nanobiotechnology, 11*, 22. doi:10.1186/1477-3155-11-22

Kelley, L. C., Lohmer, L. L., Hagedorn, E. J., & Sherwood, D. R. (2014). Traversing the basement membrane in vivo: a diversity of strategies. *J Cell Biol, 204*(3), 291-302. doi:10.1083/jcb.201311112

Kim, E., Xiong, H., Striemer, C. C., Fang, D. Z., Fauchet, P. M., McGrath, J. L., & Amemiya, S. (2008). A structure-permeability relationship of ultrathin nanoporous silicon membrane: a comparison with the nuclear envelope. *J Am Chem Soc, 130*(13), 4230-4231. doi:10.1021/ja711258w

Krishnamoorthy, G., & Wekerle, H. (2009). EAE: an immunologist's magic eye. *Eur J Immunol, 39*(8), 2031-2035. doi:10.1002/eji.200939568

Lippmann, E. S., Al-Ahmad, A., Palecek, S. P., & Shusta, E. V. (2013). Modeling the blood-brain barrier using stem cell sources. *Fluids Barriers CNS, 10*(1), 2. doi:10.1186/2045-8118-10-2

Luu, N. T., Rainger, G. E., & Nash, G. B. (2000). Differential ability of exogenous chemotactic agents to disrupt transendothelial migration of flowing neutrophils. *J Immunol, 164*(11), 5961-5969.

Lyck, R., Lecuyer, M. A., Abadier, M., Wyss, C. B., Matti, C., Rosito, M., . . . Engelhardt, B. (2017). ALCAM (CD166) is involved in extravasation of monocytes rather than T cells across the blood-brain barrier. *J Cereb Blood Flow Metab, 37*(8), 2894-2909. doi:10.1177/0271678x16678639

Martin, R., Sospedra, M., Rosito, M., & Engelhardt, B. (2016). Current multiple sclerosis treatments have improved our understanding of MS autoimmune pathogenesis. *Eur J Immunol, 46*(9), 2078-2090. doi:10.1002/eji.201646485

Martinelli, R., Zeiger, A. S., Whitfield, M., Sciuto, T. E., Dvorak, A., Van Vliet, K. J., . . . Carman, C. V. (2014). Probing the biomechanical contribution of the endothelium to lymphocyte

migration: diapedesis by the path of least resistance. *J Cell Sci, 127*(Pt 17), 3720-3734. doi:10.1242/jcs.148619

Mazzocchi, A. R., Man, A. J., DesOrmeaux, J.-P. S., & Gaborski, T. R. (2014). Porous Membranes Promote Endothelial Differentiation of Adipose-Derived Stem Cells and Perivascular Interactions. *Cellular and Molecular Bioengineering, 7*(3), 369-378. doi:10.1007/s12195-014-0354-7

Munir, H., Rainger, G. E., Nash, G. B., & McGettrick, H. (2015). Analyzing the effects of stromal cells on the recruitment of leukocytes from flow. *J Vis Exp*(95), e52480. doi:10.3791/52480

Nehilla, B. J., Nataraj, N., Gaborski, T. R., & McGrath, J. L. (2014). Endothelial vacuolization induced by highly permeable silicon membranes. *Acta Biomater, 10*(11), 4670-4677. doi:10.1016/j.actbio.2014.07.022

Neuhaus, W., Lauer, R., Oelzant, S., Fringeli, U. P., Ecker, G. F., & Noe, C. R. (2006). A novel flow based hollow-fiber blood-brain barrier in vitro model with immortalised cell line PBMEC/C1-2. *J Biotechnol, 125*(1), 127-141. doi:10.1016/j.jbiotec.2006.02.019

Pedroso, D. C., Tellechea, A., Moura, L., Fidalgo-Carvalho, I., Duarte, J., Carvalho, E., & Ferreira, L. (2011). Improved survival, vascular differentiation and wound healing potential of stem cells co-cultured with endothelial cells. *PLoS One, 6*(1), e16114. doi:10.1371/journal.pone.0016114

Reiss, Y., Hoch, G., Deutsch, U., & Engelhardt, B. (1998). T cell interaction with ICAM-1-deficient endothelium in vitro: essential role for ICAM-1 and ICAM-2 in transendothelial migration of T cells. *Eur J Immunol, 28*(10), 3086-3099. doi:10.1002/(sici)1521-4141(199810)28:10<3086::Aid-immu3086>3.0.Co;2-z

Rudolph, H., Klopstein, A., Gruber, I., Blatti, C., Lyck, R., & Engelhardt, B. (2016). Postarrest stalling rather than crawling favors CD8(+) over CD4(+) T-cell migration across the blood-brain barrier under flow in vitro. *Eur J Immunol, 46*(9), 2187-2203. doi:10.1002/eji.201546251

Sallusto, F., Schaerli, P., Loetscher, P., Schaniel, C., Lenig, D., Mackay, C. R., . . . Lanzavecchia, A. (1998). Rapid and coordinated switch in chemokine receptor expression during dendritic cell maturation. *Eur J Immunol, 28*(9), 2760-2769. doi:10.1002/(sici)1521-4141(199809)28:09<2760::aid-immu2760>3.0.co;2-n

Samuel, W., Jaworski, C., Postnikova, O. A., Kutty, R. K., Duncan, T., Tan, L. X., . . . Redmond, T. M. (2017). Appropriately differentiated ARPE-19 cells regain phenotype and gene expression profiles similar to those of native RPE cells. *Mol Vis, 23*, 60-89.

Schreiber, T. H., Shinder, V., Cain, D. W., Alon, R., & Sackstein, R. (2007). Shear flow-dependent integration of apical and subendothelial chemokines in T-cell transmigration: implications for locomotion and the multistep paradigm. *Blood, 109*(4), 1381-1386. doi:10.1182/blood-2006-07-032995

Shaw, S. K., Ma, S., Kim, M. B., Rao, R. M., Hartman, C. U., Froio, R. M., . . . Luscinskas, F. W. (2004). Coordinated redistribution of leukocyte LFA-1 and endothelial cell ICAM-1 accompany neutrophil transmigration. *J Exp Med, 200*(12), 1571-1580. doi:10.1084/jem.20040965

Shulman, Z., & Alon, R. (2012). Real-time analysis of integrin-dependent transendothelial migration and integrin-independent interstitial motility of leukocytes. *Methods Mol Biol, 757*, 31-45. doi:10.1007/978-1-61779-166-6_3

Shulman, Z., Shinder, V., Klein, E., Grabovsky, V., Yeger, O., Geron, E., . . . Alon, R. (2009). Lymphocyte crawling and transendothelial migration require chemokine triggering of high-affinity LFA-1 integrin. *Immunity, 30*(3), 384-396. doi:10.1016/j.immuni.2008.12.020

Snyder, J. L., Clark, A., Jr., Fang, D. Z., Gaborski, T. R., Striemer, C. C., Fauchet, P. M., & McGrath, J. L. (2011). An experimental and theoretical analysis of molecular separations by diffusion through ultrathin nanoporous membranes. *J Memb Sci, 369*(1-2), 119-129. doi:10.1016/j.memsci.2010.11.056

Sospedra, M., & Martin, R. (2016). Immunology of Multiple Sclerosis. *Semin Neurol, 36*(2), 115-127. doi:10.1055/s-0036-1579739

Steiner, O., Coisne, C., Cecchelli, R., Boscacci, R., Deutsch, U., Engelhardt, B., & Lyck, R. (2010). Differential roles for endothelial ICAM-1, ICAM-2, and VCAM-1 in shear-resistant T cell arrest, polarization, and directed crawling on blood-brain barrier endothelium. *J Immunol, 185*(8), 4846-4855. doi:10.4049/jimmunol.0903732

Steiner, O., Coisne, C., Engelhardt, B., & Lyck, R. (2011). Comparison of immortalized bEnd5 and primary mouse brain microvascular endothelial cells as in vitro blood-brain barrier models for the study of T cell extravasation. *J Cereb Blood Flow Metab, 31*(1), 315-327. doi:10.1038/jcbfm.2010.96

Striemer, C. C., Gaborski, T. R., McGrath, J. L., & Fauchet, P. M. (2007). Charge- and size-based separation of macromolecules using ultrathin silicon membranes. *Nature, 445*(7129), 749-753. doi:10.1038/nature05532

Takeshita, Y., Obermeier, B., Cotleur, A., Sano, Y., Kanda, T., & Ransohoff, R. M. (2014). An in vitro blood-brain barrier model combining shear stress and endothelial cell/astrocyte co-culture. *J Neurosci Methods, 232*, 165-172. doi:10.1016/j.jneumeth.2014.05.013

Tanner, K. (2012). Regulation of the basement membrane by epithelia generated forces. *Phys Biol, 9*(6), 065003. doi:10.1088/1478-3975/9/6/065003

Vandenhaute, E., Drolez, A., Sevin, E., Gosselet, F., Mysiorek, C., & Dehouck, M. P. (2016). Adapting coculture in vitro models of the blood-brain barrier for use in cancer research: maintaining an appropriate endothelial monolayer for the assessment of transendothelial migration. *Lab Invest, 96*(5), 588-598. doi:10.1038/labinvest.2016.35

Walter, F. R., Valkai, S., Kincses, A., Petneházi, A., Czeller, T., Veszelka, S., . . . Dér, A. (2016). A versatile lab-on-a-chip tool for modeling biological barriers. *Sensors and Actuators B: Chemical, 222*, 1209-1219. doi:https://doi.org/10.1016/j.snb.2015.07.110

Weksler, B. B., Subileau, E. A., Perriere, N., Charneau, P., Holloway, K., Leveque, M., . . . Couraud, P. O. (2005). Blood-brain barrier-specific properties of a human adult brain endothelial cell line. *Faseb j, 19*(13), 1872-1874. doi:10.1096/fj.04-3458fje

Winans, J. D., J. P. Smith, K., Gaborski, T., Roussie, J. A., & McGrath, J. (2015). *Membrane Capacity and Fouling Mechanisms for Ultrathin Nanomembranes in Dead-end Filtration* (Vol. 499).

Xu, H., Li, Z., Yu, Y., Sizdahkhani, S., Ho, W. S., Yin, F., . . . Qin, J. (2016). A dynamic in vivo-like organotypic blood-brain barrier model to probe metastatic brain tumors. *Sci Rep, 6*, 36670. doi:10.1038/srep36670

Figure 1

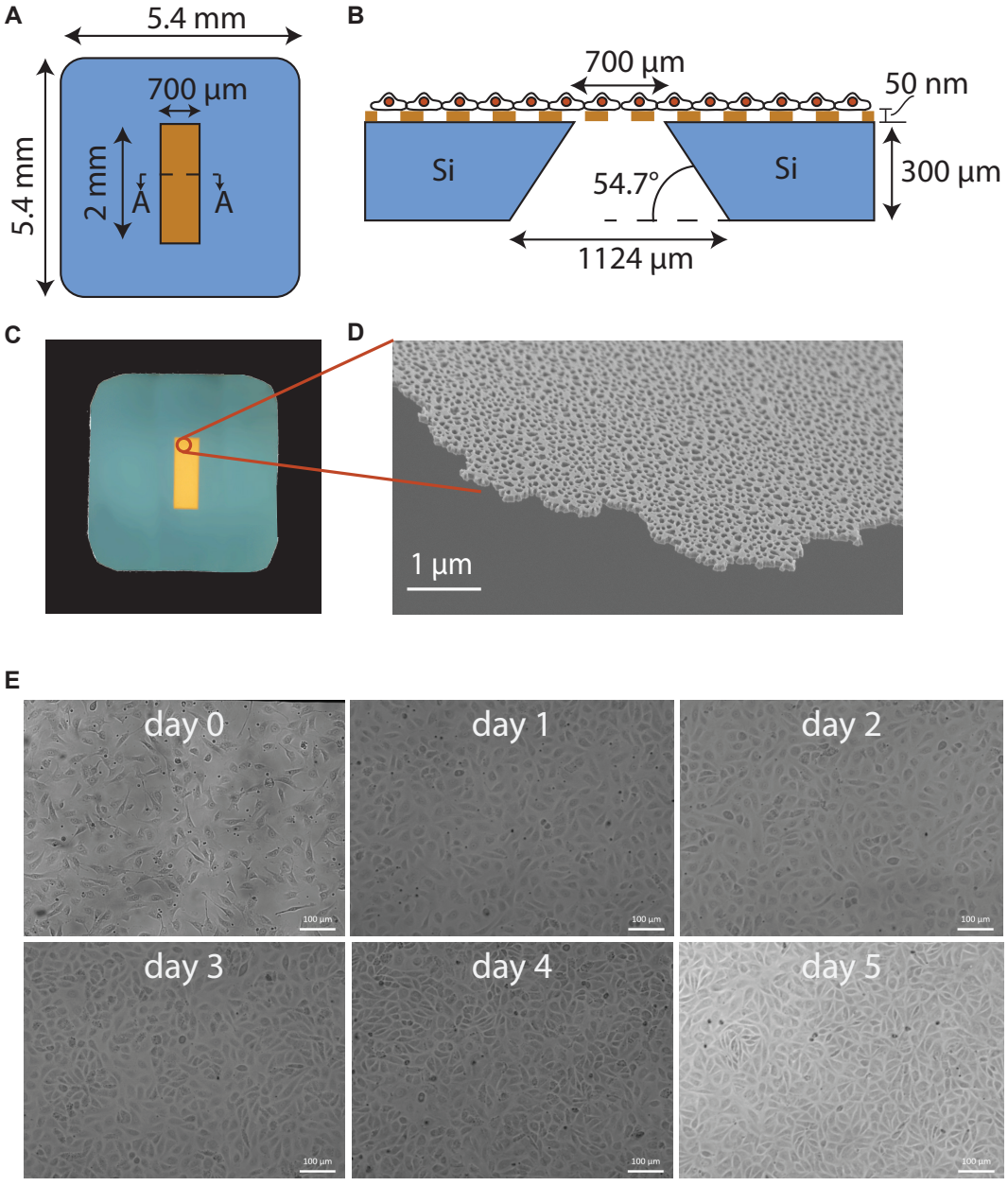
A
5.4 mm
700 µm
5.4 mm
2 mm
A
A
B
700 µm
50 nm
Si
Si
54.7°
300 µm
1124 µm
C
D
1 µm
E
day 0
day 1
day 2
day 3
day 4
day 5

Figure 2

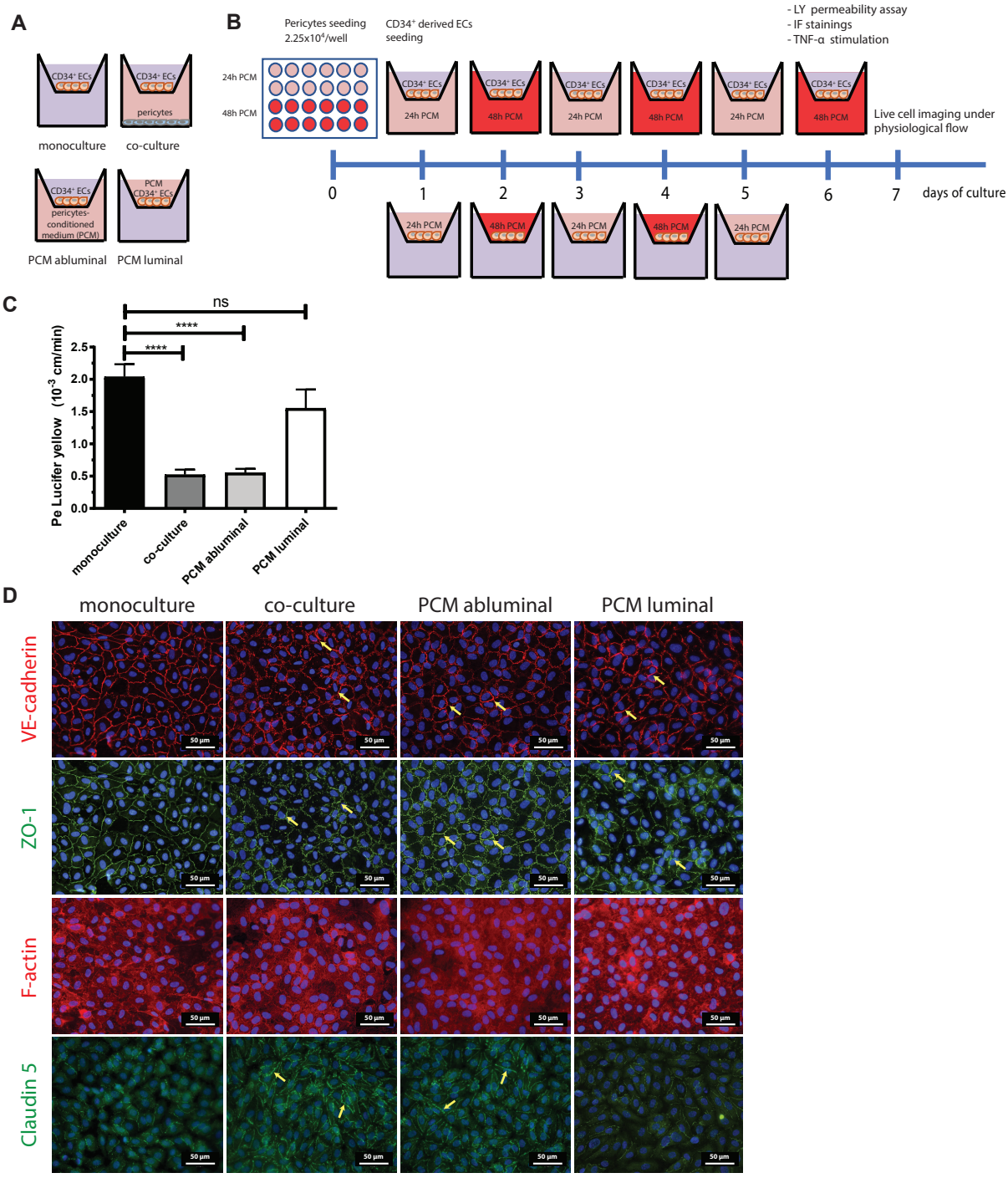
A
CD34+ ECs
pericytes
monoculture
co-culture
PCM
pericytes-conditioned medium (PCM)
PCM abluminal
PCM luminal
B
Pericytes seeding 2.25x10⁴/well
CD34+ derived ECs seeding
- LY permeability assay
- IF stainings
- TNF-α stimulation
24h PCM
48h PCM
Live cell imaging under physiological flow
0
1
2
3
4
5
6
7
days of culture
C
ns
****
****
Pe Lucifer yellow (10⁻³ cm/min)
2.5
2.0
1.5
1.0
0.5
0.0
monoculture
co-culture
PCM abluminal
PCM luminal
D
monoculture
co-culture
PCM abluminal
PCM luminal
VE-cadherin
ZO-1
F-actin
Claudin 5
50 µm

Figure 3

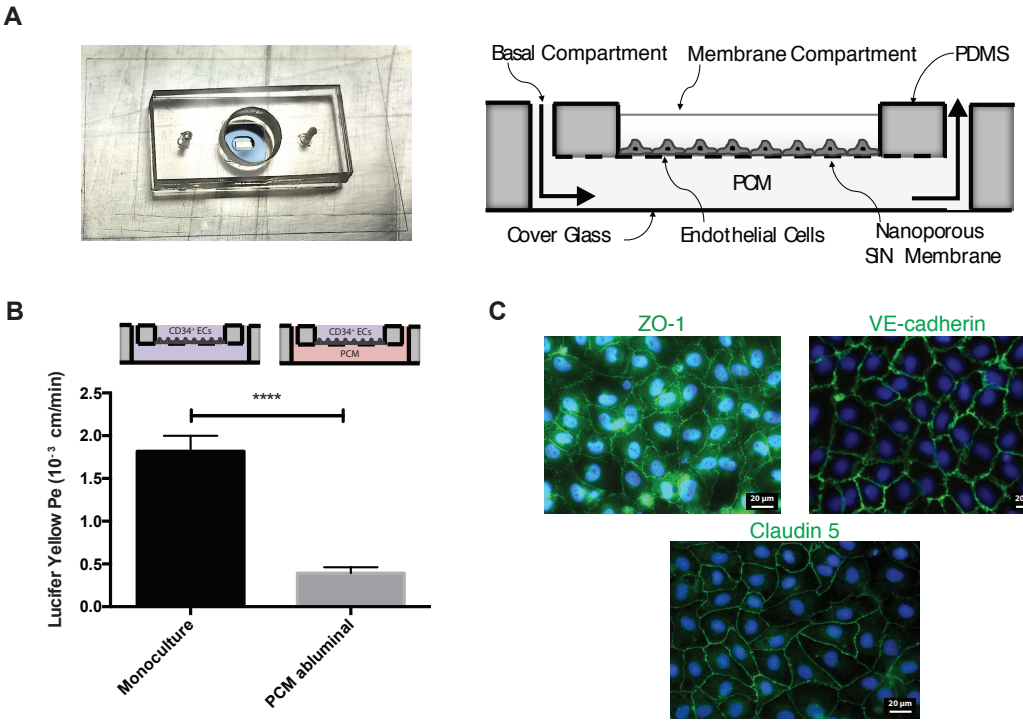
A
Basal Compartment
Membrane Compartment
PDMS
PCM
Cover Glass
Endothelial Cells
Nanoporous
SiN Membrane
B
CD34+ ECs
CD34+ ECs
PCM
****
Lucifer Yellow Pe (10-3 cm/min)
2.5
2.0
1.5
1.0
0.5
0.0
Monoculture
PCM abluminal
C
ZO-1
VE-cadherin
Claudin 5
20 µm
D
ICAM-1
ICAM-2
VCAM-1
F-actin
NS
TNF-α
20 µm

Figure 4

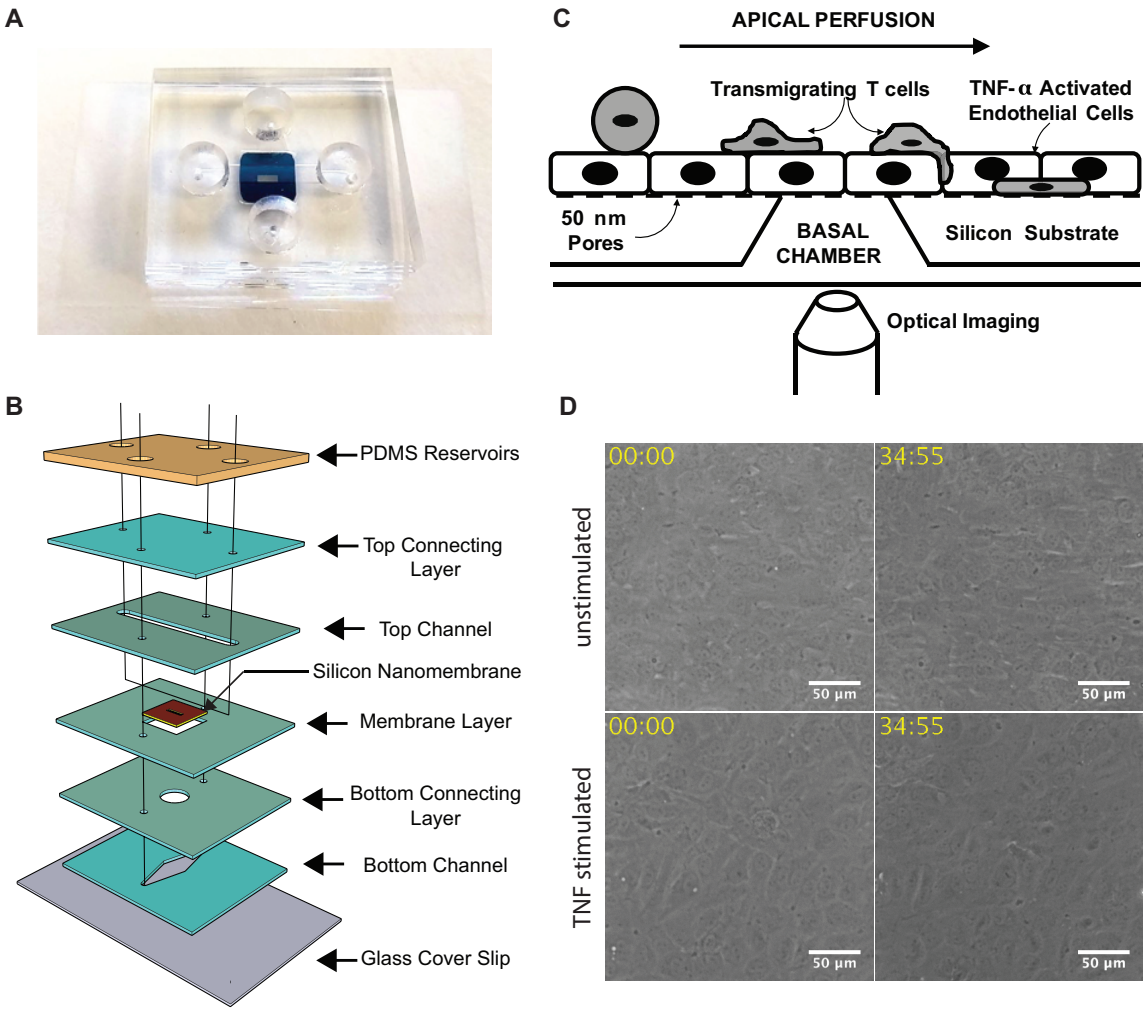
A
B
PDMS Reservoirs
Top Connecting Layer
Top Channel
Silicon Nanomembrane
Membrane Layer
Bottom Connecting Layer
Bottom Channel
Glass Cover Slip
C
APICAL PERFUSION
Transmigrating T cells
TNF-α Activated Endothelial Cells
50 nm Pores
BASAL CHAMBER
Silicon Substrate
Optical Imaging
D
unstimulated
TNF stimulated
00:00
34:55
50 µm

Figure 5

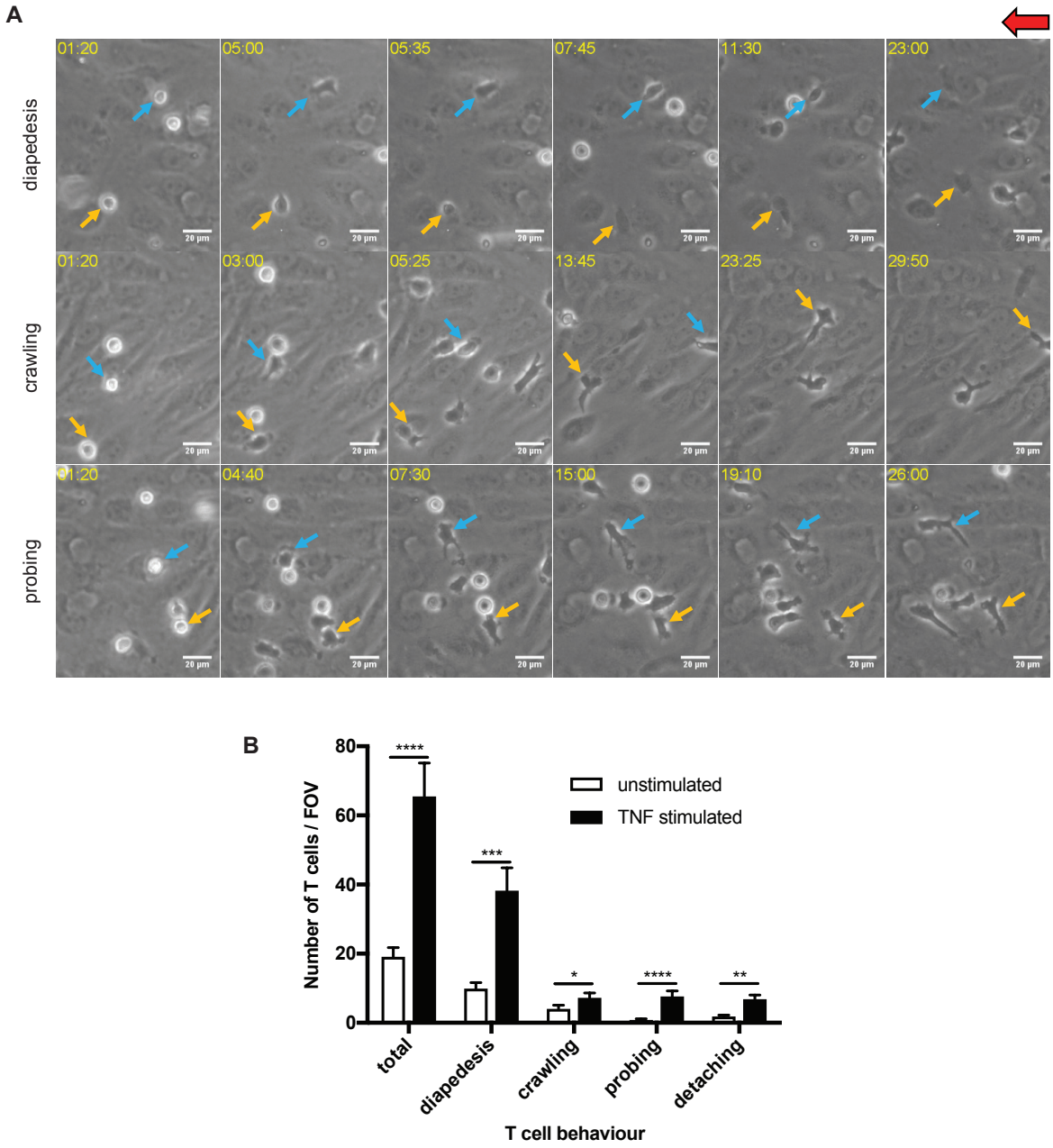
A
diapedesis
crawling
probing
01:20
05:00
05:35
07:45
11:30
23:00
01:20
03:00
05:25
13:45
23:25
29:50
01:20
04:40
07:30
15:00
19:10
26:00
20 µm
B
Number of T cells / FOV
80
60
40
20
0
****
***
*
****
**
unstimulated
TNF stimulated
total
diapedesis
crawling
probing
detaching
T cell behaviour

Figure legends

Figure 1. CD34$^+$ - derived ECs grow to confluent monolayers on the nanoporous silicon nitride membrane.

(A) Schematic of the nanoporous silicon nitride membrane used for the cell culture experiments. The free-standing membrane region is a 2 mm x 0.7 mm window in the center of a 5.4 mm x 5.4 mm membrane 'chip'. (B) The cross-sectional (A-A) schematic of the membrane. The bulk substrate consists of 300 microns of crystalline silicon, which is etched at the center to remove the bulk leaving a free standing 50 nm thin silicon nitride membrane. The manufacturing of these membranes was described before (DesOrmeaux et al., 2014). (C) Optical micrograph of the membrane chip. (D) Scanning electron micrograph of the porous membrane demonstrating the ultrathin nature and porous structure of the silicon nitride membrane (> 20% porosity in this example). (E) Phase contrast pictures of CD34$^+$ -derived ECs adhering and growing to confluent monolayers on the NPN membranes from day 0 until day 5 after plating. The CD34$^+$ ECs adhere on the NPN membrane after 1 to 2 hours and start to grow to form a confluent monolayer between 1 and 2 days of culture. Cellular density increases until day 5. Scale bar, 100 µm.

Figure 2. Induction of BBB characteristics in CD34$^+$ ECs by pericyte-conditioned medium

(A) Scheme of the different culture conditions used to test the BBB induction (B) Timeline of experimental procedures: scheme of the PCM production and luminal or abluminal administration to the CD34$^+$-derived ECs followed by Lucifer Yellow (LY) permeability assay, immunofluorescence stainings and live cell imaging under physiological flow. (C) Lucifer Yellow (LY) permeability assay: the permeability was measured across monocultures of CD34$^+$-derived ECs (monoculture), CD34$^+$ -derived ECs co-cultured with pericytes (co-culture), or pericyte-conditioned medium at the abluminal (PCM abluminal) or luminal (PCM luminal) side. Bars show means ± SEM of n= 3 independent experiments performed at least in duplicate for each condition. Statistical analysis: one-way ANOVA followed by Dunnett's multiple comparison test **** $p < 0.0001$. (D) Immunofluorescence stainings for the junctional proteins VE-cadherin (red), ZO-1 (green),

claudin-5 (green) and for F-actin (red) in $CD34^+$ -derived ECs grown in mono-culture, in co-culture with pericytes or with PCM administered at the abluminal or luminal side are shown. The pictures show a more jagged VE-cadherin and ZO-1 fluorescent staining in the co-culture and PCM conditions (arrows). The claudin 5 staining is also more important and continuous in the co-culture and PCM abluminal conditions (arrows). Scale bar, 50 µm.

Figure 3. $CD34^+$ -derived ECs grown on nanoporous silicon nitride membranes establish BLECs characteristics.

(A) Design of a "Transwell mimetic" device developed to culture $CD34^+$ -derived ECs in the membrane compartment of the NPN membrane, in close proximity to the pericyte-conditioned medium (PCM) in the basal compartment. The device is constructed from poly dimethyl siloxane (PDMS) and silicone gaskets sandwiched together using UV-ozone bonding. Note the transparent nature of the whole device in general, and specifically of the silicon membrane used to support cell growth. The schematic is shown on the right (drawn not to scale). Molecular tracers can be added to the membrane compartment and collected from the basal compartment for fluorometric analysis. (B) The permeability Lucifer Yellow (PeLY) was measured across monolayers of $CD34^+$ -derived ECs grown alone (monoculture) and $CD34^+$ -derived ECs cultured in the presence of PCM in the abluminal compartment. The values show mean ± SEM of 11 customized devices for the $CD34^+$ -derived ECs mono-cultures and 12 devices for the $CD34^+$ ECs cultured in the presence of abluminal PCM. Statistical analysis: Student's t-test ****$p < 0.0001$. (C) Immunofluorescence staining on BLECs, induced by pericyte-conditioned medium in the basal compartment, for the junctional markers ZO-1 (green), VE-cadherin (green), and claudin-5 (green). Each staining is representative of 2 independent experiment performed on 2 distinct devices, Scale bar, 20 µm. (D) Immunofluorescence staining for ICAM-1 and ICAM-2 (red), VCAM-1 (green), and F-actin (red) on BLECs unstimulated (NS) or stimulated with TNF-α for 16h. Each staining is representative of 2 independent experiment performed on 2 distinct devices. Scale bar, 20 µm.

Figure 4: Assembly of the µSiM-CVB flow system

(A) Photograph of the assembled µSiM-CVB flow system. Note the optical transparency of the device components (PDMS, silicone gaskets and silicon membrane) upon complete assembly. (B) Exploded view of the µSiM-CVB flow system. The supporting layer of the device is a thin #1.5 glass cover slip. All the silicone layers (blue/green/teal) are 300 microns thick. 'Top' and 'Bottom' channel allows the perfused media to run through the respective layers, while the 'Top Connecting Layer' and 'Bottom Connecting Layer' demarcate the top and bottom compartments respectively, and prohibit the media from leaking outside. The 'Membrane Layer' provides a framework for supporting the membrane, and is also 300 microns. The topmost layer is PDMS reservoirs, which hold the media and act as storage units. They are exposed to the outside environment in the incubator to allow for gas exchange. Similarly, all the other device components- PDMS, and the silicone gaskets are all gas-permeable and sterile. The entire device is autoclavable for sterilization. During flow set-up, the 18 gauge needles fitted with silicone tubings are inserted in the 4 holes in the Top Connecting Layer, and form a liquid-tight connection. (C) Schematic of the settings allowing the live cell imaging of the T cells-BLECs interactions under flow. T-cells are perfused on the apical (top) side of the device, which transmigrate through the endothelial cells and crawl in the subendothelial layer above the nanoporous membrane. The pores in the silicon membrane are too small (~ 50 nm) to allow crawling into the basal (bottom) compartment of the device. The working distance of the device (distance between microscope objective and T-cells) is 1.180 mm. (D) A temporal snapshot illustrating the level of resolution as well as the stability of the focus under flow has been made with several frames taken from two videos recorded with a 10x magnification (EC Plan-Neofluar 10X/0.30 Ph1). The $CD34^+$ ECs were cultured in the top channel of the flow chamber with the pericyte-conditioned medium in the bottom channel for 6 days and the $CD34^+$ ECs were stimulated or not with TNF (10 ng/mL) 16h before starting to record the videos. Th1 cells are allowed to accumulate on the BLECs monolayer at a low flow rate of 0.1 dyne/cm^2 for 4 min from the first frame after the first Th1 cells appear in the field of view, then the flow rate was set to 1.5 dyne/cm^2 for 30 min (shear phase). The pictures are showing areas without any T cells interacting with the BLECs to illustrate how we could clearly image the BLECs monolayer and how the focus remains stable from the start (00min) to the end (34min55s) of the

recording session under flow. The time is displayed on the top left of the video (min:sec format). Scale = 30 µm.

Figure 5. *in vitro* live cell imaging of the T cell-BBB interactions under flow

(A) A temporal snapshot illustrating the different T cell-BLECs interactions has been made with several frames taken from a video recorded with a 20x magnification (LD Plan-Neofluar 20X/0.4 Korr Ph2). The $CD34^+$ ECs were cultured in the top channel of the flow chamber with the pericyte-conditioned medium in the bottom channel for 6 days and the $CD34^+$ ECs were stimulated with TNF (10 ng/mL) 16h before starting to record the video. Th1 cells are allowed to accumulate on the BLECs monolayer at a low flow rate of 0.1 dyne/cm^2 for 4 min from the first frame after the first Th1 cells appear in the field of view, then the flow rate was set to 1.5 dyne/cm^2 for 30 min (shear phase). Each row is showing a specific behavior of the Th1 cells with the BLECs with the example of 2 different cells one highlighted with a blue arrow and the other one with a yellow arrow. The first row illustrates the diapedesis event where T cells start to arrest (1min20s) and then polarize and firmly adhere (5min) to the BLECs. Then the T cells start to transmigrate through the BLECs monolayer (5min35s) and take more (23min, blue arrow) or less (7min45s, yellow arrow) time to complete diapedesis. The pore size of 50 nm prevents the leukocytes from crossing the silicon membrane, and cells are trapped in the subendothelial spaces and can still be followed and identified by their darker gray shape in comparison of the BLECs monolayer (23min). The second row illustrates the crawling event where T cells first arrest (1min20s) and then polarize and firmly adhere (3min) to the BLECs. Then the T cells start to form a leading edge with a lot of small protrusions (5min25s, blue arrow and 13min45s, yellow arrow) and actively move on the BLECs against the direction of the flow until they even disappear from the field of view (13min45s, blue arrow and 29min50s, yellow arrow). The third row illustrates the probing event where T cells first arrest (1min20s) and then polarize and firmly adhere (4min40s) to the BLECs. Then the T cells remained stationary without displacing beyond a distance exceeding their own diameter and presenting the ability to greatly modulate their shape, sending a lot of dynamic cellular protrusions around them (from 7min30s to 26min). The red arrow shows the direction of flow and the time is displayed on the top left of the video (min:sec format). Scale = 20 µm.

(B) Analysis of the arrest and postarrest T-cell interactions with NS and TNF-α stimulated BLECs in the field of view of the videos recorded with a 10x magnification (example in video 1 and 2) under physiological flow (1.5 dyne/cm^2) for 30 min. T cells remaining arrested to the BLECs monolayer where quantified (total) at the end of the accumulation phase (0.1 dyne/cm2 for 4 min from the time the first T cells appear in the field of view). Then post-arrest T cell behavior on the BLECs monolayer under flow was analyzed such as each T cell was assigned to one of 4 categories as follows: diapedesis, crawling, probing and detaching. Values are means ± SEM for 10 assays for each condition. Statistical analysis: t-test * $p < 0.05$, ** $p < 0.01$, $p < 0.001$, ****$p < 0.0001$.

Video 1. Th1 cell interactions with the unstimulated BBB under flow

The BLECs were induced by growing CD34$^+$ -derived ECs in the top channel of the flow chamber with the pericyte-conditioned medium in the bottom channel for 6 days before the assay. Th1 cells are allowed to accumulate on the BLECs monolayer at a low flow rate of 0.1 dyne/cm^2 for 4 min from the first frame after the first Th1 cells appear in the field of view. After the accumulation phase at precisely 4 min 55 sec, the flow rate was set to 1.5 dyne/cm^2 for 30 min (shear phase). The dynamic T cell interactions with the BLECs monolayer under a physiological flow were recorded with a 10x magnification (EC Plan-Neofluar 10X/0.30 Ph1) with a Zeiss Axiocam MRm camera. During the recording, 1 picture was acquired every 5s and the time laps video was exported with a framerate of 30 images/s. The video shown here is repeated 3 times, the 1st run shows the full-scale video, the 2nd run is a zoom in of one area highlighting a T cell crawling (green circle) on the BLECs monolayer, and the 3rd run is a zoom in of one area highlighting T cell diapedesis (blue circle) and T cell probing (orange circle) events. The red arrow shows the direction of flow and the time is displayed on the top left of the video (min:sec format). Scale = 100 µm. The video is representative of 10 experiments and the statistical analysis of the T cell behavior is shown in the Figure 5B.

Video 2. Th1 cell interactions with the TNF stimulated BBB under flow

The $CD34^+$ ECs were cultured in the top channel of the flow chamber with the pericyte-conditioned medium in the bottom channel for 6 days and the $CD34^+$ ECs were stimulated with TNF (10 ng/mL) 16h to 20h before starting to record the video. Th1 cells are allowed to accumulate on the BLECs monolayer at a low flow rate of 0.1 dyne/cm^2 for 4 min from the first frame after the first Th1 cells appear in the field of view (accumulation phase until 4min55s). After the accumulation phase of precisely 4 min 55 sec, the flow rate was set to 1.5 dyne/cm^2 for 30 min (shear phase). The dynamic T cell interactions with the BLECs monolayer under a physiological flow were recorded at a 10x magnification (EC Plan-Neofluar 10X/0.30 Ph1) with a Zeiss Axiocam MRm camera. During the recording, 1 picture is acquired every 5s then the video is exported with a framerate of 30 images/s. The video is repeated 3 times, the first run shows the full-scale video, the second run is a zoom in of one area highlighting T cells crawling (green circles) and detaching (purple circles) and the last run is a zoom in of one area highlighting diapedesis (blue circles) and probing (orange circles) events. The red arrow shows the direction of flow and the time is displayed on the top left of the video (min:sec format). Scale = 100 μm. The video is representative of 10 and the statistical analysis of the T cell behavior is showed in the Figure 5B.

Supplementary Material

Table 1. List of commercially available cell culture filter inserts tested to adapt the human *in vitro* BBB model established from $CD34^+$EC co-cultured with bovine pericytes as described (Cecchelli et al., 2014) to our established custom-made flow chamber system exactly as described (Enzmann et al., 2013). The table lists the technical problems encountered for each cell culture filter insert and gives reference to Supplementary Videos provided allowing to judge the image quality of BLECs on the respective filter systems.

Supplementary video 1. Flow chamber adaptation of the human BBB model using 6 well hanging inserts, 0.4 µm pore size, PTFE, coated, Millipore, Sevelen, Switzerland (1^{st} device listed in the supplementary table 1). BLECs are detaching under the flow, and the lack of transparency of the filter makes the imaging of the cell difficult.

Supplementary video 2. Flow chamber adaptation of the human BBB model using 6 well hanging inserts, 0.4 µm pore size, PTFE, coated, Corning Incorporated, NY, USA (5^{th} device listed in the supplementary table 1). T cell on top of BLECs not clearly visible under the flow.

Supplementary video 3. Flow chamber adaptation of the human BBB model using 6 well hanging inserts, 0.4 µm pore size, PET Corning Incorporated, NY, USA (6^{th} device listed in the supplementary table 1). T cell on top of BLECs not visible under the flow. Imaging disturbed by the membrane pores brightness, respect to the membrane insufficiently transparent.

Supplementary video 4. Flow chamber adaptation of the human BBB model using 6 well hanging inserts, 0.4 µm pore size, PET Greiner, Huber & Co. Ag Reinach Switzerland, (7^{th} device listed in the supplementary table 1). T cell on top of BLECs not visible under the flow. Imaging disturbed by the membrane pores brightness, respect to the membrane insufficiently transparent.

Supplementary Table 1

Insert description	Experiments Performed	Limitations of inserts
1. 6 well standing inserts, low wall, 0.4 µm pore size, PTFE Millipore, Sevelen, Switzerland (Enzmann et al. 2013)	Cell growth on coated filter Membranes: Matrigel, laminin, gelatine and rat tail collagen	BLECs do not adhere on this filters
2. 6 well standing inserts, high wall, 0.4 µm pore size, polycarbonate Millipore, Sevelen, Switzerland	Cell growth Light Microscopy	Filter membrane is not transparent
3. 6 well standing inserts high wall 0.4 µm pore size mixed cellulose esters Millipore, Sevelen, Switzerland	Cell growth Light Microscopy	Filter membrane is not transparent
4. 6 well hanging inserts, 0.4 µm pore size, polycarbonate Corning Incorporated, NY, USA	Cell growth Light Microscopy	Filter membrane is not transparent
5. 6 well hanging inserts, 0.4 µm pore size, PTFE coated Corning Incorporated, NY, USA	Cell growth Light Microscopy In vitro flow assay	Filter membrane is insufficiently transparent
6. 6 well hanging inserts, 0.4 µm pore size, PET Corning Incorporated, NY, USA	Cell growth Light Microscopy In vitro flow assay	Filter membrane is insufficiently transparent
7. 6 well hanging inserts, 0.4 µm pore size, PET Greiner, Huber & Co. Ag Reinach Switzerland	Cell growth Light Microscopy In vitro flow assay	Filter membrane is insufficiently transparent

Supplementary Figure 1

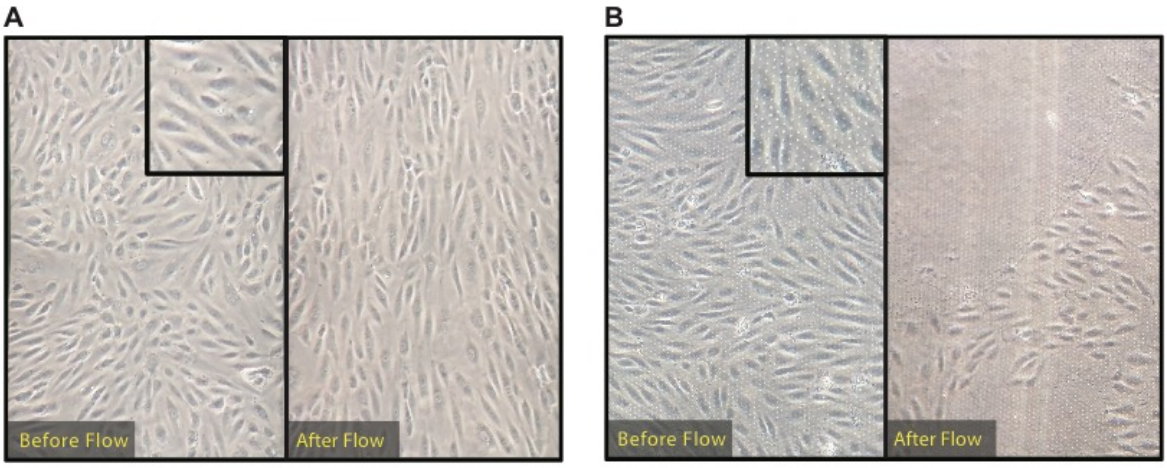

Figure S1. Comparison of the NPN and SiO_2 membranes endothelial cell attachment properties under flow

(A) Human umbilical vein endothelial cells (HUVECs) are grown on nanoporous silicon nitride (NPN) for 24 hours under static condition (left panel), and were later exposed to ~9-10 dynes/cm^2 of shear stress of fluid flow for another 24 hours (right panel). Inset represents a zoomed in image of the cell monolayer without any noticeable pore distribution on the membrane substrate. (B) HUVECs were grown under similar static conditions on 3 µm pores silicon dioxide membranes (left panel) followed with identical shear stress exposure. Notice the visible presence of 3 µm pores during phase imaging as observed in the inset (magnified view). Within 2 hours of shear introduction, there is over 60% cell loss from the membrane substrate as shown in the right panel.